The Thesis Committee for Abhishek Goel
Certifies that this is the approved version of the following thesis:

Electrochemical Deposition of Metal Ions in Porous Laser Sintered Inter-metallic and Ceramic Preforms

APPROVED BY
SUPERVISING COMMITTEE:

Supervisor:

David L. Bourell

Joseph J. Beaman Jr

Electrochemical Deposition of Metal Ions in Porous Laser Sintered Inter-metallic and Ceramic Preforms

by

Abhishek Goel, B.Tech

Thesis

Presented to the Faculty of the Graduate School of

The University of Texas at Austin

in Partial Fulfillment

of the Requirements

for the Degree of

Master of Science in Engineering

The University of Texas at Austin

December 2010

To my grandfather, *for all the love and affection*

To my father, *for always believing in me*

To my mother, *for encouraging me all the time*

To my teachers, *for all the knowledge instilled in me*

To Lord Ganesha*, for "Shubh Labh Riddhi Siddhi"*

and of course

To my little sister, *for her invariable cheerfulness*

Acknowledgements

I would like to express my sincere gratitude to Dr. David L. Bourell for being a wonderful and motivating advisor. Words cannot explain the contentment, pride and pleasure I gained in working for him. Without his guidance and encouragement, this research would never have been possible. I would also like to thank Dr. Joseph J. Beaman Jr. for his advice throughout my graduate school and time spent in reading this thesis. I would also like to thank National Science Foundation for their financial support for this research work. Without their continued support, I would not have been able to pursue this work and contribute to the world of engineering.

A good portion of this research involved working with hands and I have to thank Mark Phillips and Curtis Johnson for helping me with the equipment and experimental setup. I want to thank Fred Rothhauser for finding whatever I needed in the building. I also have to thank Rosalie Foster and David Justh for their superb administrative skills.

Anand Kumar Singh and Vikram Devaraj have listened to my "bakar" all the time and have helped me find a solution. Daniel Worthington, Kaushik Alayavalli, Kumaran Chakravarty, Phani Vallabhajosyula, Ryan Newcomb and numerous other colleagues have made invaluable contributions to my research. Sahil has been a wonderful roommate and has always been patient with me. I will always remember the "good times" spent in "Chaupal" with Abhinav, Himanshu and Sahil.

I would like to thank all the professors and staff from IIT, Kharagpur for believing in me and instilling in me solid foundations of mechanical and manufacturing engineering. Vishal, Mukul, Nishant, 'Kauaa', Robin, Sudhanshu and Savi have been my pillars of strength all of these years and I am grateful for their support when I needed it most. I am glad and thankful that what started six years ago is still continuing.

I want to thank Pink Floyd, Dream Theater and Porcupine Tree, whose wonderful music helped me sustain my concentration at work. The Flying Saucer, JP's Java and Mozart's was where I spent a lot of my free time. My Macbook, iPhone and "Netflix" have been invaluable additions to my life.

Vinay Agarwal has been like an elder brother to me away from home. I would like to thank him for his continued invaluable support. I want to thank Gunjan, Abhishek and Mohit, who have always been there when I needed them the most.

My parents have always permitted me to do "whatever" I want to do and have supported every decision I have ever made. From the bottom of my soul and the depths of my heart, I want to thank you for everything. The encouragement, love, affection which my parents and sister have showered on me makes me believe that I am the luckiest man alive!

ABHISHEK GOEL

The University of Texas at Austin

December 2010

Abstract

Electrochemical Deposition of Metal Ions in Porous Laser Sintered Inter-metallic and Ceramic Preforms

Abhishek Goel, M.S.E

The University of Texas at Austin, 2010

Supervisor: David L. Bourell

Selective laser sintering (SLS) is a commercial, powder-based manufacturing process that produces parts with complicated shape and geometry based on a computer solid model. One of the major drawbacks of SLSed inter-metallic and ceramic parts is their high porosity because of the use of binder system. High porosity results in poor mechanical, electrical and thermal properties of the preform and hence renders it unsuitable for various applications. This thesis attempts to infiltrate SLSed preforms by carrying out electrochemical deposition of metal ions inside the interconnected pore network. One of the major benefits of carrying out this novel process is low processing temperature as opposed to existing methods such as melt infiltration. Low temperature reduces both energy consumption and associated carbon-footprint and also minimizes undesirable structural changes. Both conductive and non-conductive preforms may be electrochemically infiltrated, and MMCs produced by this method have potential for use in structural applications.

Table of Contents

Chapter 1: *Introduction* 1

Selective laser sintering 1

Indirect selective laser sintering 2

Candidate material systems 3

State of the art infiltration methods 8

Electrochemical Deposition 12

Candidate Plating Systems 15

Need for this research 23

Chapter 2: *Experimental* 26

Selective Laser Sintering 26

Electrochemical Deposition 36

Chapter 3: *Results* 43

Porosity Measurement 43

Deposition: SEM and EDS 45

Energy Considerations 54

Chapter 4: *Discussion* 55

Porosity Measurement 55

Deposition: SEM and EDS 55

Energy Considerations 58

Chapter 5: *Summary, Conclusions and Future Work* 60

Summary 60

Conclusions 61

Future Work 61

Bibliography 63

Vita 67

List of Tables

Table 1. Properties of sintered silicon carbide 5
Table 2. Properties of pure graphite 7
Table 3. Properties of Durite AD 332A (Phenolic) 27
Table 4. Properties of silicon carbide powder 30
Table 5. Parameters used for silicon carbide sintering 31
Table 6. Properties of GS 150E graphite powder 33
Table 7. Parameters used for graphite sintering 35
Table 8. Constituents of electroless nickel plating bath 37
Table 9. Constituents of electrolytic nickel plating bath 38
Table 10. Specification of Shurflo GCBN23V gear pump 41
Table 11. Pychnometer porosity measurements of SiC LS brown parts 43
Table 12. Pychnometer porosity measurements of graphite LS brown parts 43
Table 13. Weight percentage of nickel obtained after each deposition process ... 54
Table 14. Energy comparison for various kinds of deposition process 54

List of Figures

Figure 1. Schematic of selective laser sintering process 2

Figure 2. Structure of 4H- α-SiC..... 4

Figure 3. Side view of the layer structure of graphite 6

Figure 4. Schematic of gas pressure infiltration process 9

Figure 5. Schematic of squeeze casting infiltration process..... 10

Figure 6. Schematic of pressure die infiltration process 11

Figure 7. Schematic of chemical vapor infiltration process 12

Figure 8. Schematic of an electrolytic deposition process 13

Figure 9. Distorted A6 indirect SLSed tool steel part vacuum infiltrated with cast iron 25

Figure 10. SEM image of the phenolic resin powder..... 26

Figure 11. Differential Scanning Calorimetry of phenolic resin 28

Figure 12. Roller system for powder mixing..... 29

Figure 13. SEM image of the silicon carbide powder..... 30

Figure 14. SEM image of the synthetic graphite powder..... 34

Figure 15. Modified deposition: (a) cylindrical graphite cathode(b) rectangular graphite (SiC part) or copper (graphite part) cathode 39

Figure 16. (a) Schematic of forced diffusion process (b) Laser sintered graphite sample..... 40

Figure 17. Forced diffusion deposition setup 41

Figure 18. SEM image showing porous network in the SiC brown part..... 44

Figure 19. SEM image showing porous network in the graphite brown part..... 44

Figure 20. SEM image of a SiC preform after carrying out electroless nickel deposition 45
Figure 21. SEM image of a SiC part after carrying out electrolytic nickel deposition 45
Figure 22. SEM image of a SiC part after modified deposition with cylindrical cathode..... 46
Figure 23. SEM image of a SiC part after modified deposition with rectangular cathode..... 46
Figure 24. SEM image of a graphite part after modified deposition with rectangular copper cathode 47
Figure 25. SEM image of a graphite part after forced electroless deposition 47
Figure 26. EDS spectrum for electroless deposition on SiC preforms..... 48
Figure 27. EDS spectrum for electrolytic deposition on SiC preforms..... 48
Figure 28. EDS spectrum for modified deposition on SiC preforms with cylindrical cathode..... 49
Figure 29. EDS spectrum for modified deposition on SiC preforms with rectangular cathode..... 49
Figure 30. EDS spectrum for modified deposition on graphite preforms with rectangular copper cathode..... 50
Figure 31. EDS spectrum for forced electroless deposition on cylindrical disk graphite preforms..... 50
Figure 32. EDS map showing distribution of nickel after electroless deposition on SiC 51
Figure 33. EDS map showing distribution of nickel after electrolytic deposition on SiC..... 51

Figure 34. EDS map showing distribution of nickel after modified deposition with cylindrical cathode on SiC 52
Figure 35. EDS map showing distribution of nickel after modified deposition with rectangular cathode on SiC 52
Figure 36. EDS map showing relative distribution of nickel after modified deposition with rectangular copper cathode on graphite 53
Figure 37. EDS map showing relative distribution of nickel after forced electroless deposition on graphite 53

Chapter 1: *Introduction*

SELECTIVE LASER SINTERING

Selective laser sintering (SLS) is a powder-based layer-additive manufacturing process (Deckard, 1986) used to make models for design testing, patterns for investment casting and small lots of functional parts. Selective laser sintering is a solid freeform fabrication (SFF) process, the production of freeform solid objects directly from a computer model without part-specific tooling or human intervention (Bourell, 1990).

Powder is spread as a thin layer approximately 125 microns thick. A computer-controlled laser selectively fuses the powdered material by scanning cross-sections generated from a 3D digital description of the part (e.g. CAD model) on the surface of a powder bed. After each cross-section is scanned, the powder bed is lowered by one layer thickness, a new layer of material is applied on the top, and the process is repeated thousands of times to create an entire part with virtually unlimited geometric complexity. Alternatively, for inter-metallic and ceramic parts, the powder may be mixed with a transient binder which melts under the scanning laser beam and is removed or converted in a post-processing step known as burnout. The low melting point of the binder permits rapid green part formation which can then be burnt out to obtain the brown part (Subramanian, 1995). A schematic of the SLS process is shown in Figure 1.

The advantages of SLS are best utilized in the manufacture of parts with complex geometry in low production runs. There is considerable potential for application in actual production parts, but there are issues with high-performance metallic part production. While several commercial machines for direct metal processing have been developed and marketed in the last two years, the machines and associated metal powder are extremely expensive and build times are 5 times higher compared to the polymers. An alternative

approach is to SLS-process green parts composed of a metal or ceramic powder mixed with a transient binder. The material may be run in relatively low-cost and high-speed polymer SLS machines.

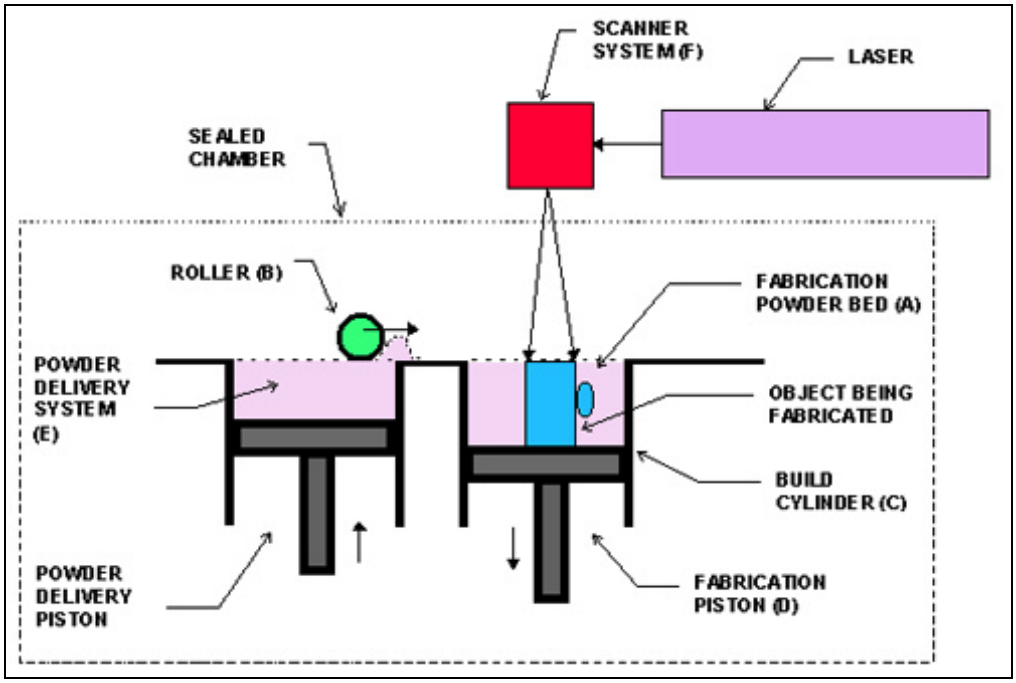

Figure 1. Schematic of selective laser sintering process

INDIRECT SELECTIVE LASER SINTERING

In direct laser sintering, powder bed temperature is raised up to the fusing point of the sintering material to minimize thermal gradients. In indirect laser sintering, this strategy is difficult to fulfill especially for material systems with high melting point. The melting point of silicon carbide is around 2700°C and that of graphite is above 3000°C. The high melting point indicates that a high laser power from the heating source is required to fuse the powder particles together. This is not possible to achieve since the maximum power output from the currently used SLS machine is 50 Watt. That is why it is necessary to carry out the indirect SLS of high melting ceramics and inter-metallics by

mixing them with a thermosetting polymer which acts as a binder. The binder should have a low melting point and high bonding strength. The binder serves as the connecting media in the green part to maintain its geometric integrity for subsequent post-processing. Thermosetting binders such as furan resin, epoxy resin, phenolic resin, unsaturated polymer, etc. are used in various applications in the molding industry. Among these, phenolic resins have a better thermal stability and flame resistance. Phenolic resins can also yield up to 70% of the carbon residue after thermal treatment. Due to these superior properties and high carbon yield from pyrolysis, phenolic resin was chosen to be the binder for SLS of graphite and silicon carbide. Phenolic resins are usually made from condensation polymerization of phenol and formaldehyde because of which they are also known as phenol formaldehyde resins. Under inert atmosphere with high temperature treatment, phenolic resin can provide high vitreous carbon yield which contributes to the structural integrity and electrical conductivity of the preform.

CANDIDATE MATERIAL SYSTEMS

Silicon Carbide

Silicon carbide also known as carbonundum occurs in nature as an extremely rare mineral moissanite. Silicon carbide exists in about 250 crystalline forms. α-SiC is the most commonly occurring polytype of silicon carbide and has an hexagonal structure as shown in Figure 2. (Madar, 2004). Pressureless sintering of silicon carbide is an attractive densification process for producing components with complicated geometries at low cost. The strength loss in silicon carbide is minimal at high temperatures. The good strength retention of silicon carbide at high temperature and good oxidation resistance has increased interest in sintering of silicon carbide (Dutta, 1984).

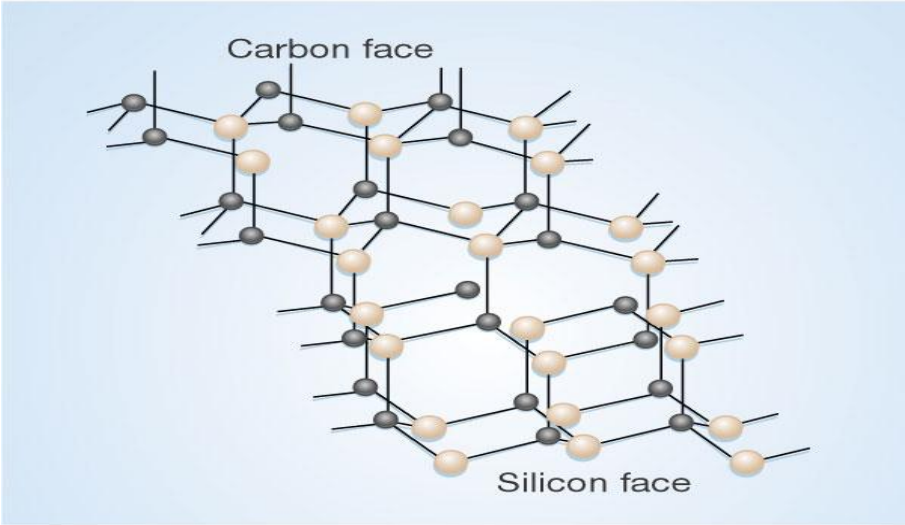

Figure 2. Structure of 4H- α-SiC

Silicon carbide is a ceramic with material properties that make it desirable for many applications but also very difficult to manufacture. Conventional manufacturing processes such as hot pressing, sintering, chemical vapor deposition (CVD) and chemical vapor infiltration inflict severe geometrical constraints on the parts and are also time-consuming and expensive. Many of these issues associated with these manufacturing routes can be eliminated with the implementation of indirect selective laser sintering process. Indirect selective laser sintering has proved to be very effective in fabrication of silicon carbide parts. This material is of interest where high temperature strength and stability are required, and where wear and corrosion are issues (Stevinson, 2006). The applications of silicon carbide include electronics processing wafer carriers and boats, kiln components, pump seal rings, nozzles and wear parts.

Approximately 87% of the bonds in silicon carbide are covalent, which imparts high mechanical strength to sintered parts (Somiya, 1991). Silicon carbide is brittle and its low fracture toughness limits its application in structural components. Sintered silicon

carbide have high strength and toughness at high temperatures and recently, they have widespread use as a wear resistant material in mechanical components. Some of the properties of sintered silicon carbide are shown in Table 1.

Table 1. Properties of sintered silicon carbide

Property	Units	Value
Density	g/cc	3.10 - 3.25
Hardness	Vickers HV	2.38e3 - 2.63e3
Flexural Strength	ksi	53 - 58.5
Compressive Strength	ksi	442 - 487
Elastic Modulus	psi 10^6	56.6 - 59.5
Thermal Conductivity	W/m °C	90 - 110
Electrical Resistivity	μohm-cm	1e9 - 3.16e10

Graphite

Graphite is largely produced from petroleum coke or pitch during graphitization process. The temperature to convert amorphous carbon to graphite is around 3000°C (Mantell, 1979). Graphitization is the process that involves rearrangement and displacement of layer planes to form 3-dimensional ordering of crystalline structures. Each plane is linked to adjacent planes by weak Van der Waals forces. The weak Van der Waals forces between individual layers allow them to slide over one another easily, making graphite an ideal lubricant. The electrical conductivity of graphite mainly comes from delocalizing of π electrons across the hexagonal atomic sheets of carbon, and the conductivity parallel to these sheets is greater than that perpendicular to the sheets. The

electrical conductivity of pure graphite is around 1.5 x 10^3 S/cm. The hexagonal structure of crystalline graphite is shown in Figure 3.

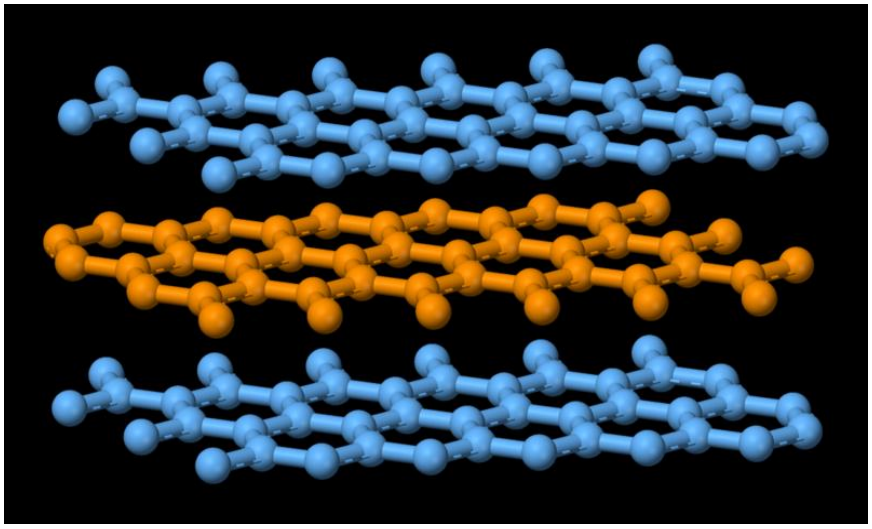

Figure 3. Side view of the layer structure of graphite

Graphite is brittle and has poor machinability therefore, indirect laser sintering of graphite is an attractive process for making low cost inter-metallic components with complex geometry. Due to its low density and chemical inertness, graphite is used for making bipolar plates for direct methanol fuel cells. The bipolar plates made using laser sintering of graphite show excellent mechanical and electrical properties (Alayavalli, 2010). Some of the properties of pure graphite are shown in Table 2.

Table 2. Properties of pure graphite

Property	Units	Value
Density	g/cc	2.2 - 2.26
Hardness	Vickers HV	4 - 50
Flexural Strength	ksi	0.754 - 6.09
Compressive Strength	ksi	6.24 – 50.8
Elastic Modulus	psi 10^6	1.45 – 3.63
Thermal Conductivity	W/m °C	80 - 240
Electrical Resistivity	μohm-cm	34.7 – 6.03e3

Post processing: Infiltration

In case of inter-metallic or ceramic preforms, following green part production, the parts are post-processed, usually by conventional solid-state sintering or by infiltration to close off open porosity and densify the part. Various researchers have developed infiltration systems including infiltrants of silicon into a silicon carbide SLS part (Evans, 2005) and alloy white cast iron into a tool steel SLS preform (Vallabhajosyula, 2008). These infiltration approaches require high temperature to melt the infiltrant and rely on wetting kinetics to draw the infiltrant into the part. In the research described here, the desire is at ambient temperature to fill effectively the open porosity of an SLS green part by electrochemical deposition. Inter-metallic and ceramic preforms are typically 50-60% dense with virtually all porosity being open or connected. The average pore size is typically the order of the powder size, approximately 30-60 μm. The average pore size in the solid phase sintered SiC preform has been seen to vary from 1 μm to 100 μm with an average pore size of 55 μm, approximated to be equal to the particle size. Variation of

electrical (Koh, 1973) and mechanical properties (Wang, 1984) of the preform with porosity is given by the following equations.

$$\frac{J}{J_0} = \frac{1-\varepsilon}{1+n\varepsilon^2}$$

$$\frac{E}{E_0} = \exp(-b\varepsilon)$$

$$\frac{\sigma}{\sigma_0} = \exp(-b\varepsilon)$$

where, J / J_0 is the ratio of porous conductivity to fully densified conductivity, ε is the fractional porosity, n is sensitivity to the presence of pores, E / E_0 is the ratio of porous modulus to fully densified modulus, σ / σ_0 is the ratio of porous strength to fully densified strength and b is the tortuosity factor which depends on the pore shape.

STATE OF THE ART INFILTRATION METHODS

Melt infiltration is a liquid state method of composite materials fabrication in which porous ceramic performs are soaked in a molten metal which fills the pores (Toy, 1990). The driving force of the melt infiltration process is either spontaneous due to the capillary force of the porous preform or an external pressure (such as gaseous, mechanical, etc.) is applied to the liquid metal matrix. Examples of metal matrix composites (MMCs) made using the melt infiltration technique are SiC/Al composites, W-Cu composites and Si-Mo alloy in carbon preforms.

Gas pressure infiltration (GPI) is process for preparation of composite materials where molten material is infiltrated into the pores of a preform under the influence of high gas pressure (Chiou, 1991). Figure 4 (Kopeliovich, 2009) shows a schematic of the gas pressure infiltration process. Heating is carried out under vacuum to melt the matrix material, and then a porous preform is immersed into the melt. The infiltration is then carried out at high pressure, and a chemical or a mechanical bond is formed between the

constituents. Si/Al composite is a very good example of MMC manufactured using the gas pressure infiltration method.

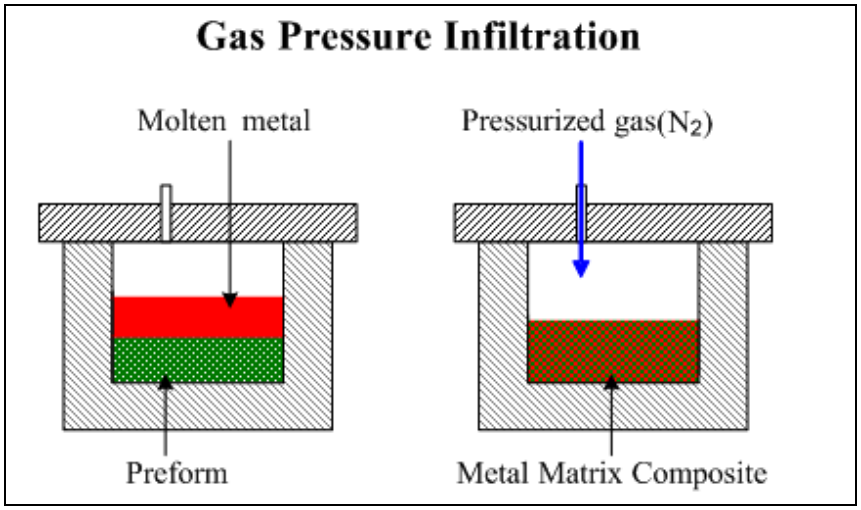

Figure 4. Schematic of gas pressure infiltration process

Squeeze casting infiltration is a forced infiltration method of liquid phase fabrication of metal matrix composites, using a movable mold part (ram) for applying pressure on the molten metal and forcing it to penetrate into the ceramic preform, placed into the lower fixed mold part (Ghomashchi, 2000). The method is widely used for manufacturing automotive engine pistons from aluminum alloy reinforced by alumina short fibers. The schematic of the squeeze casting infiltration process is shown in Figure 5 (Dieringa, 2005).

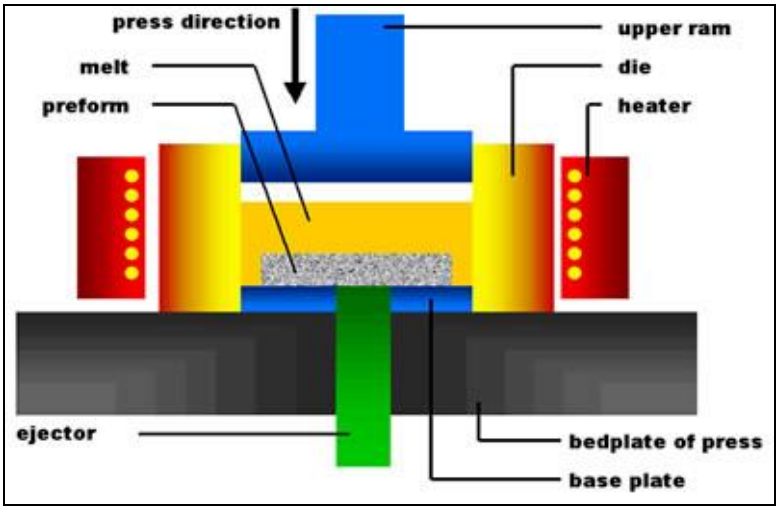

Figure 5. Schematic of squeeze casting infiltration process

Pressure die infiltration is a forced infiltration method of liquid phase fabrication of metal matrix composites, using a die casting technology. The preformed dispersed phase is placed into a die (mold) which is then filled with a molten metal entering the die through a sprue and penetrating into the preform under the pressure of a movable piston (plunger) as shown in Figure 6 (Kopeliovich, 2009). The moving solid piston causes turbulent flow of the melt upstream the preform (Mortensen, 2000). Aluminum composite materials are made using pressure die infiltration process.

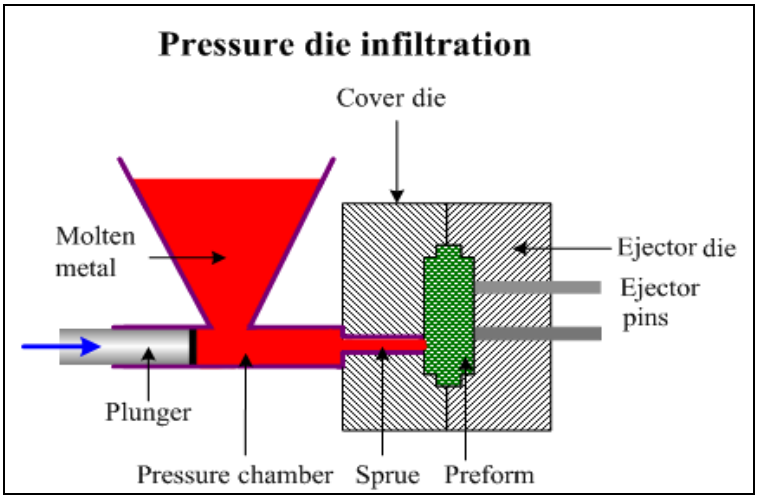

Figure 6. Schematic of pressure die infiltration process

Chemical vapor infiltration is an infiltration process in which reactant gases diffuse into an isothermal porous preform and form a deposit as shown in Figure 7 (Kopeliovich, 2009). Deposited material is a result of chemical reaction occurring on the pores' surface. The deposition fills the space between the fibers, forming composite material in which the matrix is the deposited material and the dispersed phase is the fibers of the preform (Besmann, 1990). Chemical vapor infiltration (CVI) is similar to chemical vapor deposition in which deposition forms when vapor gases react on the outer surface of the substrate. CVI is widely used for fabrication of silicon carbide matrix composites reinforced by silicon carbide continuous (long) fibers.

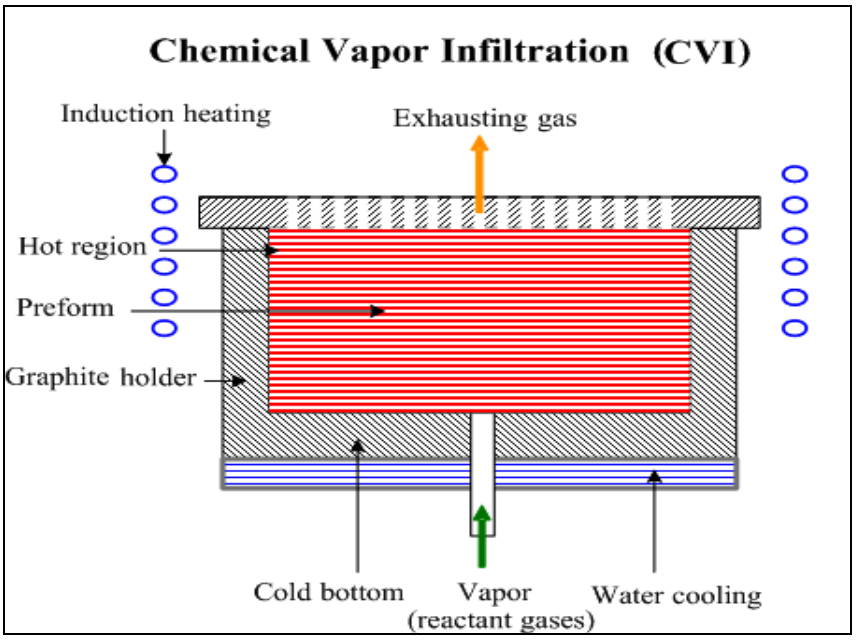

Figure 7. Schematic of chemical vapor infiltration process

ELECTROCHEMICAL DEPOSITION

Electrochemical deposition of metals and alloys involves the reduction of metal ions from aqueous, organic or fused-salt electrolytes. The reduction of metal ions in the aqueous solution is represented by:

$$M_{sol}^{n+} + ne \rightarrow M_{lattice}$$

The deposition phenomena associated with the above mentioned equations consist of four important facets (Paunovic, 2006): the metal-solution interface that consists of a metal and an aqueous ionic solution acts as the locus of the deposition process; the kinetics and mechanism of the deposition process which are related to statistical and quantum mechanics; the understanding of the nucleation and growth process of the metal lattice such as formation of monolayers and multilayers; and, growth of coherent bulk deposit. It is also important to keep track of the structure and nature of the deposit using

various surface and bulk analysis techniques. The schematic of the electrochemical deposition process is shown in Figure 8.

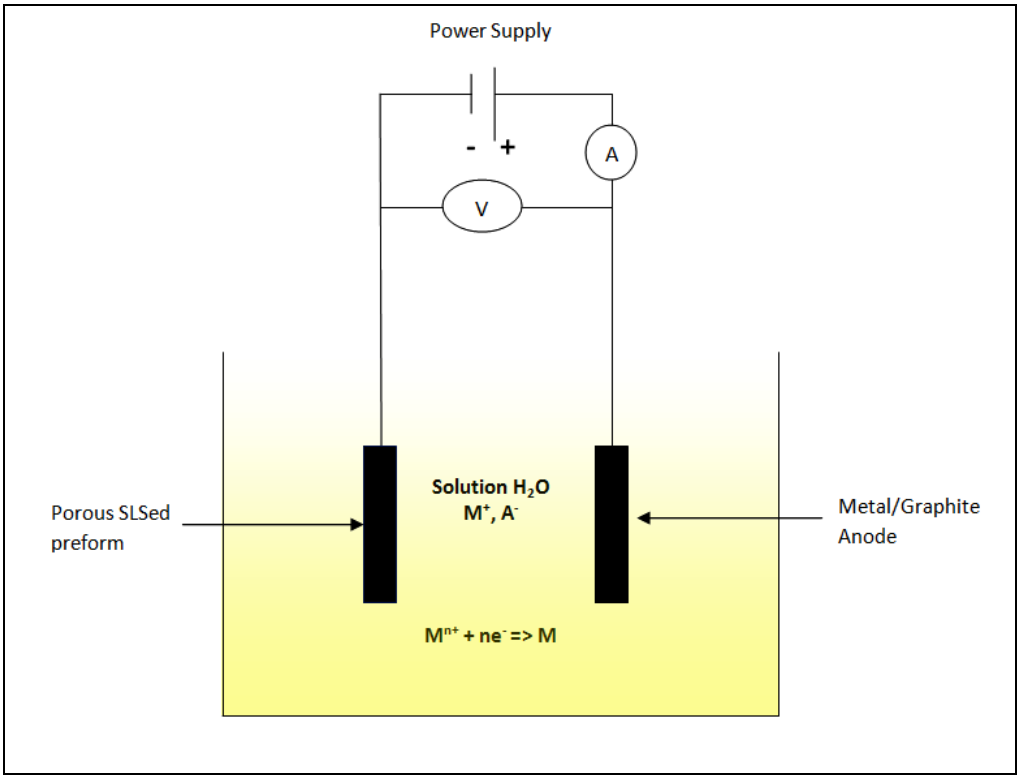

Figure 8. Schematic of an electrolytic deposition process

To reduce one mole of a given metal from a metal ion with the valence charge of $n+$, n moles of electrons are required. That is, the total cathodic charge used in the deposition, Q, is the product of the number of gram moles of the metal deposited, m, the number of electrons taking part in the reduction, n, Avogadro's number, N_a (the number of atoms in a mole), and the electrical charge per electron, Q_e. Thus, the following equation gives the charge required to reduce m moles of metal (Lou, 2006):

$$Q = mnN_a Q_e$$

$N_a Q_e = F$, where F is Faraday's constant, therefore, $m = Q/nF$. On the other hand, the total charge used in the deposition can be obtained as the product of the current, I , and the time of deposition, t (in seconds) if the deposition current is held constant. Or, if the current varies during the deposition, the total charge is given by:

$$Q = \int Idt$$

The weight of the deposit, W (in grams), thus can be obtained by multiplying the number of moles of metal reduced with the atomic weight, M_w , of the deposited metal:

$$W = \frac{M_w}{nF} \int Idt$$

Ideally, the deposition thickness δ (in cm) can be solved by the equation,

$$\delta = \frac{W}{\rho A} = \frac{M_w}{nF\rho A} \int Idt$$

Where, ρ is the density of the metal to be deposited (gm/cc) and A is the area of deposition (cm^2).

The deposition distribution along the depth of the pore depends on the polarization factor ξ as the ratio of interfacial reaction rate to the diffusion rate of nickel inside the porous network (Xu, 2006). The polarization factor is a dimensionless parameter that depends of several critical parameters such as bulk concentration of Ni^{2+} ions, diffusion coefficient of Ni^{+2} ions, overpotential and exchange current density. Hence the major factor to be taken into account is the reduction of rate of deposition on the pore surface and higher diffusion rates inside the interconnected porous network. This can be achieved by controlling the polarization factor and inhibiting the deposition on the pore surface by using additives such as sodium allylsulfonate or coumarin. To increase

the rate of diffusion of ions inside the porous network, external pressure may be applied to the electrolyte to force it through the preform. The pressure drop and the remaining porosity can be measured using Darcy's law.

CANDIDATE PLATING SYSTEMS

Copper Plating

Electrodeposition of copper is widely used in the fabrication of micro-components in electronic devices (Zhang, 2008). Copper plating deposits have various functional, protective and decorative applications. Copper deposits are good thermal shock absorbers and act as thermal expansion barriers in multi-coating systems. Due to its softness, it helps in reducing corrosion failure from cracking caused by physical deformation of the part. Copper plating is also used as a final finish for decorative applications. Copper deposits generally get stained or tarnished when exposed to atmosphere, that is why they often need an overcoating of lacquer or another corrosion-resistant finish (Davis, 2001).

Copper can be deposited from both electrolytic and electroless electrolytes that are acidic or alkaline in nature. One of the most popular alkaline copper bath is copper cyanide bath. They produce uniform coating thickness and are easily controllable. They also produce best relative thickness distribution over all current densities i.e. have a good macro-throwing power. However, because of hazard and waste management issues, non-cyanide systems have replaced copper cyanide systems. They require more precise control and surface preparation compared to cyanide systems. Copper sulphate is the most widely used non-cyanide copper plating system. Acid based systems are more commonly used in electroforming, electrorefining and decorative plating. Acid based plating baths contain copper in bivalent ion form and have poorer macro-throwing power and non-uniform metal coating thickness. One the other hand, they have a good micro-

throwing power and hence they are widely used in filling trenches and vias for semiconductor applications.

Electroless copper plating was widely used in 1950s for plated-through-hole printed wiring boards. Major components of an electroless copper plating solution are metal salt and a suitable reducing agent. Since, copper salts are insoluble at pH below 4, complexing and buffering agents are necessary to act as a chelating compound and maintain and regulate the pH of the solution. Surface preparation is also necessary since, electroless deposition reaction takes place only on catalytic surfaces. One of the major advantages of electroless copper plating is that it can be used for both conductive and non-conductive surfaces. Electrodeposited copper is also widely used in multi-coating systems such as copper-nickel-chromium system. The cost of copper coating is generally higher for non-cyanide baths when compared to cyanide baths because they require better process control and use of brightening, levelling and wetting agents. Electroless copper plating is also more expensive compared to electrolytic plating.

Nickel Plating

Nickel plating has been used extensively for decorative, engineering and electroforming purposes because it is quite easy to tailor the properties of the electrodeposit by varying the composition of the electrolyte and operating parameters. Nickel plating is widely used for decorative applications because of their bright and glossy appearance. Nickel plating is also quite popular in engineering applications because of their good wear and corrosion resistant properties. Unlike, copper deposits, nickel deposits do not get tarnished on exposure to environment and hence do not require any protective overcoat on its surface.

Nickel can be deposited from both electrolytic and electroless baths. The two most popular solutions used to deposit nickel for engineering applications are Watts solution and nickel sulphamate bath. Nickel sulphamate solutions are widely used in electroforming because of their high rates of deposition, low internal stress of the deposits and high macro-throwing power. Nickel sulphamate has a high solubility because of which sulphamate baths have higher concentration of nickel which in turn permits lower operating temperature and higher plating rates (Bari, 1994). Nickel sulphamate solutions are more expensive compared to nickel sulphate or nickel chloride because of its high preparation and purification costs. Watts bath is relatively inexpensive, easy to control and capable of being used with high current densities. Good quality nickel deposits can be produced from Watts solution which have high corrosion resistance and best throwing power.

Electroless nickel plating has been one of the extensively used plating techniques for LIGA microstructures and through-hole filling for semiconductor applications. The major components of the electroless nickel plating are source of nickel cation and reducing agent. Complexing agents and buffering agents are used to control the properties of the solution and maintain uniform deposition. Electroless nickel plating is generally carried out at higher temperatures because heat serves as the source of energy. The electroless solution also needs to be continously agitated to ensure uniform deposition rate. Nickel plating process is easily controllable when compared to copper electrodeposition. Waste management and health hazards are also reduced in case of nickel plating since nickel plating solutions are less corrosive and toxic when compared to copper plating baths.

Electroless Deposition

The concept of electroless infiltration is derived from electroless deposition. It is a non-galvanic type of plating method that involves several simultaneous reactions in an aqueous solution, which occur without the use of external electrical bias (Zhao, 1998). The reaction is accomplished when hydrogen is released by a reducing agent, normally sodium hypophosphite, and oxidized thus producing a negative charge on the surface of the part. The most common electroless plating method is electroless nickel plating.

The chemical deposition of nickel metal using hypophosphite as the reducing agent has an advantage over the displacement deposition since it meets the redox potential requirements without consuming the anode substrate. Electroless plating is the term used to describe method of plating without the application of external electric current. Electroless plating is generally characterized by selective reduction of metal cations at the surface of the catalytic substrate immersed in the aqueous solution of the metal ions. The chemical and physical properties of the nickel deposit depend on its composition which in turn depends on the composition and operating conditions of the electroplating bath (Mallory, 1991). Major components of an electroless nickel plating bath are: (1) source of nickel ions, (2) reducing agent, (3) complexing agent, (4) buffering agent and (5) energy.

Surface pre-treatment is an essential step in electroless deposition. Non-catalytic surfaces have to be activated i.e. made catalytic, prior to electroless deposition. Activation is performed by generating catalytic nuclei on the surface of non-catalytic material (Paunovic, 2006). The porous microchannels differ with respect to the cations they let pass through them. Activation coupled with sensitization makes the surface conductive and attachment of the cations easier. It aids in formation of covalent bonds between the ions and the deposition surface. Activation makes the surface more reactive

without addition of material and removes the oxide layers in case of electrochemical deposition. Sensitization improves the rate of adsorption of reducing agent on the surface. Activation and sensitization with tin and palladium leads to the formation of Sn-Pd clusters on the surface of the pore walls. The nucleation process produces small Pd catalytic sites dispersed on the pore wall surface, which are less than 10 Å in diameter (Marton, 1968). The Pd particles adsorbed on the surface are surrounded by Sn^{4+} ions, which need to be removed by solubilizing it in NaOH or HCl, to expose the Pd particles. This way, Sn-Pd clusters render the surface conductive to subsequent plating.

Nickel sulphate is the most preferred source of nickel cations. Other nickel salts such as chlorides and acetates are used for limited applications due to their high cost. Moreover, chloride anions also have deleterious effects on the deposit properties for several applications. The ideal source of nickel ions is the nickel salt of hypophosphorus acid. Nickel hypophosphite eliminates addition of sulphate anions and minimizes the build up of alkali metal ions while replenishing the reactants consumed during the deposition process.

Most commonly used reducing agents in nickel plating are, sodium hypophosphite, sodium borohydride, hydrazine and dimethylamine borane. All these reducing agents contain two or more reactive hydrogens which help in nickel reduction resulting due to catalytic dehydrogenation of these reducing agents. Several theories have been proposed which discuss the reducing mechanism in the nickel deposition reaction such as atomic hydrogen acting as a reductant, hydride transfer mechanism and coordination of hydroxyl ions with hexaquonickel ion. Hypophosphite salts are preferred over other reducing agents since they can reduce metals such as copper, silver and nickel without phosphorus codeposition.

Complexing agents are used to make the deposition potential more negative in order to prevent spontaneous chemical reaction between the plating ion and the cathode. Another important function of the complexing agent is the regulation and maintenance of free nickel ion in the solution. Complexing agents coordinates to a nickel ion through an oxygen or nitrogen atom. Some of the most commonly used complexing agent in electroless nickel plating are, sodium citrate (tetradentate ligand), sodium acetate (monodentate ligand) and sodium succinate (bidentate ligand).

Formation of H^+ ions from water is a common phenomena in electroplating. The change in pH of the solution as a result of formation of H^+ ions depend on the buffering agent. Buffering agent is a substance or a mixture of substances that adjusts the pH of a solution. The function of a buffer is to drive an acidic or basic solution to a certain pH state and maintain it. The capacity of a buffering agent is determined by measuring the amount of acid (H^+) required to change the pH by a certain amount. Buffering agents can either be weak acid or weak base that would comprise a buffer solution. A buffering agent sets up this concentration ratio by providing the corresponding conjugate acid or base to stabilize the pH of that which it is added to. The resulting pH of this combination can be found by using Le Chatelier's principle:

$$pH = log_{10} \frac{[A^-]}{[HA]}$$

where, A is the anion of the base and HA is the weak acid. Some of the common buffering agents used in electroless nickel plating are, ammonium chloride, ammonium sulphate, succinic acid and hydroxyacetic acid.

The energy to an electroless plating process is supplied in the form of heat. Temperature is the measure of heat (energy) content of an electroplating solution.

These components of the bath are taken in appropriate proportions to prepare the aqueous solution, and the preform to be infiltrated is dipped in the bath and stirred for several hours (Oliver, 1988). The proportion of the salts and the time of operation depend on the type of metal to be infiltrated. Because of the non-conductive nature of the non-metallic preforms, they have to be first activated and then sensitized to make them conductive (Jain, 2009). One of the major drawbacks of the electroless infiltration technique is that it is a very slow process, and the metal can deposit completely on the surface of the perform, thereby inhibiting the infiltration of metal ions into the porous network.

Electrolytic Deposition

The principles of electrolytic infiltration are similar to electrolytic deposition wherein an electric current is used to facilitate deposition. Here an ionic metal is supplied with electrons to form a non-ionic coating on a substrate. A common system involves a chemical solution with the ionic form of the metal, an anode (positively charged) and finally, a cathode (negatively charged) where electrons are supplied to produce a film of non-ionic metal. Unlike the electroless method, a reducing agent is not required. The external electric field supplies electrons to reduce the metal ions to metals (Kanani, 2004).

The most commonly used electrolyte solution for electrolytic deposition of nickel is Watts bath. Watts bath uses a combination of nickel sulphate and nickel chloride. The combination of various sources of nickel ions allows for a variety of electrodeposit characteristics. Nickel sulphate is the most inexpensive source of nickel ions and sulphate anions have a very little effect on the deposit properties. The concentration of nickel sulphate is higher in case of application that require bright electrodeposits and is

lower for applications where throwing power is needed. Nickel chloride is good for anode corrosion and increases the conductivity of the plating solution. The concentration of nickel chloride is usually varied depending on the desired properties of the electrodeposit.

Boric acid is a very important constituent of Watts bath. It is added to nickel electroplating solutions as a buffer, to regulate and maintain the pH of the solution. Boric acid is added to the bath as this controls and reduces the changes in pH, thus preventing the precipitation of hydroxides. Boric acid is generally effective in the pH range of above 3 and therefore, it is not very useful in aerospace applications. Overall, it helps to keep nickel ions in the solution, improve the quality of the deposit and increases the operating range of the electrolyte.

Electrochemical Infiltration: Theory and Feasibility

The reaction of ceramics (SiC) and inter-metallics (graphite) with refractory metals at high temperature leads to the formation of silicides and carbides, respectively. Nickel (+2) ions have ionic radii in the range 0.065-0.073 nm, and its crystal radii vary in the range 0.079-0.087 nm (Biggar, 1969). Ions with smaller crystal radius have a higher charge density, and the higher charge density attracts more water of hydration. Thus, the smaller the crystal radius, the lower is the mobility of the ion in water. The ions move with their hydration shell in aqueous solutions where the water molecules surround the nickel cations. The ions can move across a porous membrane through various mechanisms. One such mechanism is electro-neutral diffusion which is passive diffusion of positively charged and negatively charged ions depending on the ionic concentrations (Rubinstein, 1990). The activation (opening of ion channels) and sensitization (addition of hydrophilic salts to a solution to ease flocculation of electrolyte) of SiC preforms makes it easier for transport of ions through its porous network to occur. Electro-neutral

diffusion occurs in the case of electroless infiltration, but this process is very slow when compared to electro-osmotic diffusion or electrophoretic diffusion where an addition electric field is applied to enhance the mobility of ions (Streckert, 1997). The flow of ions will stop at an equilibrium condition where the electric potential difference across the membrane comes to zero. To keep the ions moving such that all the pores are closed off or the interior walls of the pores are completely deposited by nickel ions, an external electric field needs to be applied. Various modes of transport of ions that can occur in this case can be electrophoresis, electroosmosis and electrodeionization. This latter mechanism is attractive for interporosity network deposition in SLS preforms because the deposition initiates at the electrode which may be placed in the center of an SLS preform. As deposition progresses, metal ions are fed to the solid-electrolyte interface electrophoretically. Deposition of solid then initiates in the central region of the SLS preform porosity network and works its way out as the solid deposition fills the pore structure. This has the potential to force the liquid electrolyte out of the preform uniformly rather than trapping it into micropores, resulting in a low porosity, high integrity product. In this research, The brown part is then infiltrated by dipping it in a bath containing a metallic salt as an electrolyte. Metal ions diffuse into the porous network of the brown preform where they combine with a counter electron flow resulting in metallic deposition within the pore network (Chen, 2003 and Duck, 2004).

NEED FOR THIS RESEARCH

The objective of this research is to establish a scientific understanding for electrochemical infiltration of selective laser sintered (SLS) preforms. This represents the major scientific barrier to development and maturing of a new manufacturing route for creating low-cost metal-infiltrated composites with complex geometry at room

temperature. One of the major advantages of electrochemical infiltration is the lower processing temperature, normally room temperature. Low temperature reduces both energy consumption and associated carbon footprint. It also minimizes undesirable structural change (Saleh, 2004). The results of this research will enable facile, low-cost production of metal matrix composites (MMCs) with complex geometry from commercially important materials such as silicon carbide-nickel (SiC-Ni), graphite-nickel (G-Ni) and also even nickel-nickel (Ni-Ni). A specific part example is fuel cell bipolar plates (G-Ni).

As mentioned previously, various other infiltration techniques such as CVI and melt infiltration are carried out at high temperature which produces potentially undesirable chemical and structural changes after the infiltration process. Unfortunately, these are very slow and costly processes and/or result in the case of fiber infiltration in an incomplete filling of the gaps between the fibers in the tows (Sen, 2008). In high temperature infiltration, the melt can react with the SiC preform and can have a reinforcing effect on the carbon fibers. Because of the softening of the residual silicon, the strength of these melt infiltrated composites decreases at elevated temperature (Esfehanian, 2007). The melting point of nickel is approximately 1450°C, and to prevent the melt from reacting with the preform it is necessary that the temperature of the melt be lower than 1500°C -1600°C. Figure 9 shows some of the distorted parts which might occur due to undesirable structural and chemical changes in vacuum melt infiltration process (Vallabhajosyula, 2008). Alternatively, in the room temperature process, ions transport through a three-dimensional porous network and become deposited on the interior walls of the pores. This does not lead to any structural change in the solid. Certain undesirable chemical changes can be produced by the electrolyte or gases trapped inside, but these can be driven out of the structure just by heating the preform at a

temperature of about 200-300°C. The transport of ions inside the porous structure depends on a number of factors such as their concentration in the electrolyte, ionic mobility and crystal radius and diffusion coefficient (Hasegawa, 2004).

Figure 9. Distorted A6 indirect SLSed tool steel part vacuum infiltrated with cast iron

The current research will result in facile, low-cost production of structural parts. This will result in expanding the knowledge of solid freeform fabrication and especially SLS technology. Parts built using SLS technology find applications in various areas such as fabrication of circuit components, one-off models for medical application and functional test parts. One of the major drawbacks of non-polymeric SLS technology has been high porosity. This research enables production of high-density parts without any undesirable structural and chemical changes. The proposed work represents a truly novel method in infiltration. This work would enable faster transition of SLS from rapid prototyping to rapid manufacturing technique. This would prove to be more useful in fabrication of parts with complex geometry and smaller dimensions.

Chapter 2: *Experimental*

SELECTIVE LASER SINTERING

Since this research aims at post-processing of laser sintered inter-metallic and ceramic preforms, the parts were made using DTM Sinterstation 2000 by 3D systems. In this chapter the experimental methods beginning with pre-processing of SLS powder mixture, SLS part fabrication, post-processing of the preforms, porosity measurements, electrodeposition and SEM characterization are discussed in details.

Figure 10 shows the SEM image of the phenolic resin, Durite AD 332A, obtained from Hexion Speciality Chemicals, Inc. and the properties (from datasheet) of the phenolic resin is given in Table 3.

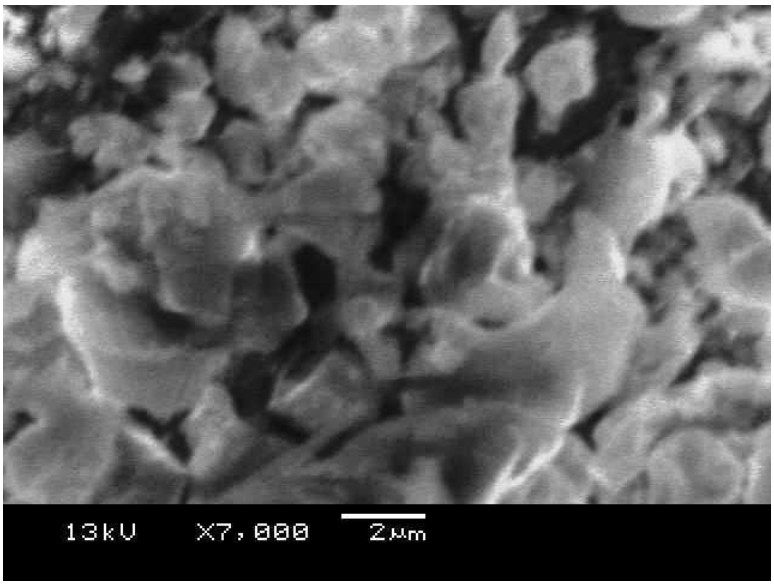

Figure 10. SEM image of the phenolic resin powder

Table 3. Properties of Durite AD 332A (Phenolic)

Property	Value
Hot plate cure, 150°C	60-90 sec
Hexa Content	9.5-10.5%
Particle Size	98-100% thru 200 mesh
Cost	~$4.85/lb

A Perkin Elmer DSC7 calorimeter was used to carry out the Differential Scanning Calorimetry (DSC) analysis of the phenolic resin. The DSC was carried out in the nitrogen atmosphere with the heating rate of 2°C/min. Figure 11 shows the DSC curve for phenolic resin. The first endothermic peak corresponds to melting of novolac resin while the second broad peak corresponds to heat of solution of hexamine in the molten resin (Burns, 1967). The only exothermic peak in the graph represents the cross-linking mechanism of novolac resin and hexamine which occurs around 155°C. Based on the DSC results the part bed temperature was set to be 60°C for graphite and 75°C for silicon carbide.

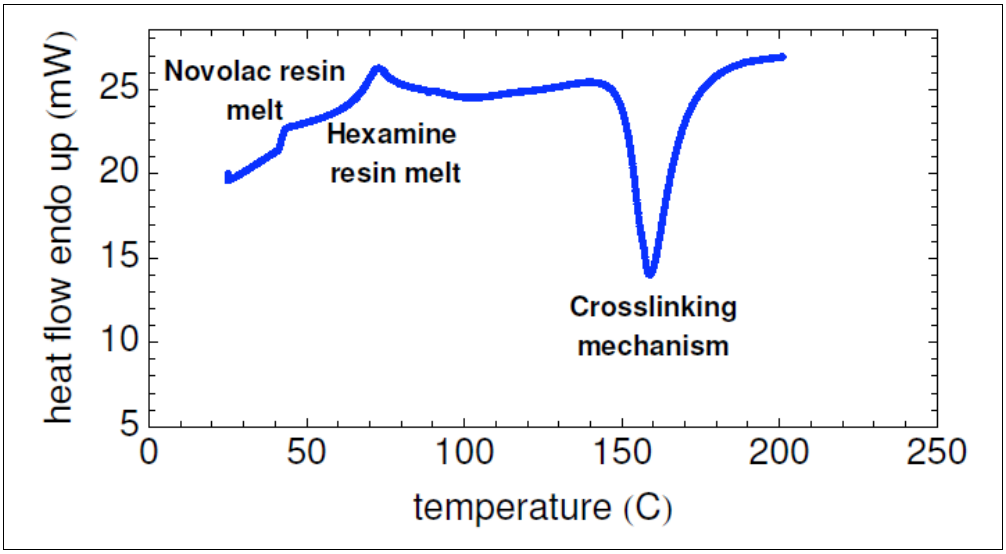

Figure 11. Differential Scanning Calorimetry of phenolic resin

Powder Preparation

Powder mixing is essential in determining the quality of the SLS parts. Non-uniform mixing of powder can lead to defects or voids in the parts, especially in liquid phase sintering. Uniform mixture minimizes the extent of anistropic shrinkage and promotes bonding strength distribution within the parts. The powder was mixed using a roller system as shown in Figure 12. The material system was blended in jar-like containers from US Stoneware with cylindrical alumina pellets as the grinding media. The jar was filled one-third with grinding media and one-third with the powder mixture to ensure proper mixing. The RPM of the roller was kept at a moderate value to minimize the segregation of the powder particles. The mixing time was approximately 5 hours, and after mixing, the alumina media was removed from the powder using a sifter.

Figure 12. Roller system for powder mixing

SLS: Silicon Carbide

Commercially available 180 grit size (avg. ~ 80 μm) silicon carbide powder from Industrial Supply, Inc. was used to make preforms for infiltration. Figure 13 shows an SEM image of the silicon carbide powder. The properties (from datasheet) of the silicon carbide powder is given in Table 4.

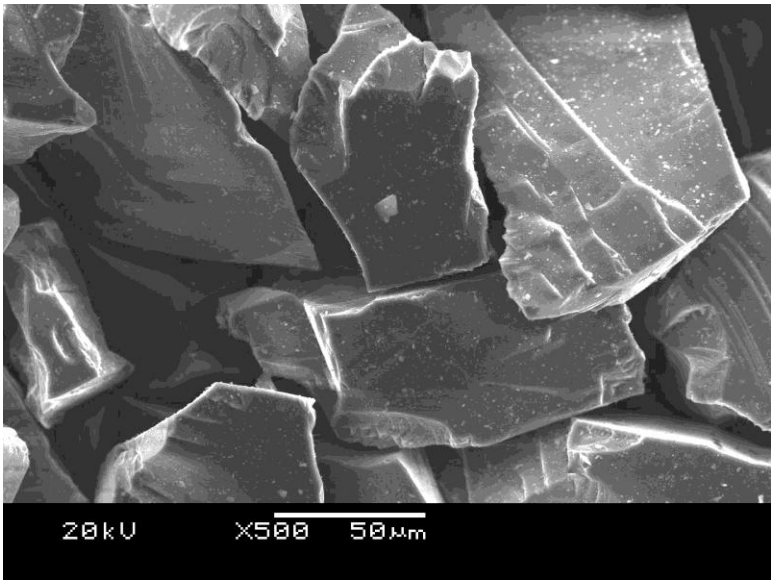

Figure 13. SEM image of the silicon carbide powder

Table 4. Properties of silicon carbide powder

Property	Value
Specific gravity	3.20
Knoop Hardness (100 scale)	2480
Particle Size	98-100% thru 120 mesh
Cost	~$0.80/lb

Computer models for the 25 mm cubic samples were generated using ProEngineer Wilfire 3.0, and the .stl files obtained were loaded onto the Sinterstation 2000 software. Shrinkage of parts during high temperature phenolic burnout was taken into account while generating these CAD models. The powder mixture was prepared by mixing silicon carbide and phenolic resin in the ratio 10:1 by weight. The powder mixture was blended inside ball milling jars and allowed to mix for 6-8 hours at moderate speed. The mixed batch of powder was sifted to eliminate large sized particles and the grinding media and

then the powder was loaded into both the feed bins of the sinterstation. Laser sintering commenced after a warm-up period in which layers of powder were rolled onto the part bed prior to sintering, generally to a thickness of 10 mm. The operating parameters used for sintering are tabulated in Table 5.

Table 5. Parameters used for silicon carbide sintering

Parameter	Values
Powder composition	100 wt% SiC and 10 wt% phenolic resin
Laser power	10 W
Outline laser power	4 W
Scan speed	1.3 m/s
Beam diameter	450 μm
Scan spacing	76.2 μm
Layer thickness	101.2 μm
Part bed temperature	75°C
Feed Bin temperatures	47°C
Process gas	Nitrogen

On completion of the laser sintering, loose powder was gently brushed from the green parts. Unsintered powder from the part bed and from the overfill bins was swept back into the feed bins and reused for subsequent runs. Green parts were weighed on a Fisher Scientific A-160 scale prior to post-processing.

Post Processing: Silicon Carbide

Post processing of the green parts consisted of two steps. At first they were infiltrated with epoxy at room temperature and then burnt out in a high-temperature furnace in vacuum. The vacuum furnace processing converted the binder to carbon (brown part creation).

At 70°C phenolic begins to soften and does not cross-link until 155°C. The parts slumps if an intermediate form of support is not used in this temperature range. Room temperature epoxy infiltration was included as a processing step to stabilize the part shape. BJB TC-162 A/B epoxy, chosen for its high temperature working rasnge (up to 177°C when post-cured) and relatively low viscosity, was mixed with xylene in a 1:1 volume ratio to further reduce its viscosity. Diluting the epoxy was necessary to prevent phenolic outgases from becoming trapped within the part during binder volatilization and causing it to burst, and also to accelerate infiltration of the green parts. Silicon carbide green parts were placed in a shallow aluminum foil pan containing the epoxy mixture for approximately two minutes or until complete infiltration occurred. The parts were dried in vacuum for two days and then post-cured in a standard lab oven. The temperature profile for post curing was: 66°C for 1.5 hours, 121°C for 2 hours, 149°C for 1 hour and 177°C for 1 hour.

After the green parts were obtained, these parts were burnt out in a Yokogawa UP550 programmable high-temperature, vacuum furnace. The furnace uses several graphite elements along with a digital controller to precisely supply the required heat into the chamber to maintain uniform temperature. It has the maximum heating capacity of up to 2000°C. The furnace chamber can be vacuumed and backfilled with various inert gases for atmosphere controls throughout the programmed temperature profile.

The temperature profile was heating at 180˚C/hr from room temperature to 200˚C, then at 30˚C/hr to 500˚C and then at 300˚C/hr to 800˚C for brown part generation, then to 1400˚C at 250˚C/hr and finally to 1650˚C at 500˚C/hr. After this, the furnace was cooled naturally. The furnace was backfilled with argon and then returned to vacuum to before heating to ensure negligible oxygen pressure. During processing, argon gas was pulsed through the furnace chamber to drive out byproducts of phenolic decomposition. The slow temperature ramp from 200°C to 500°C was employed to allow sufficient time for phenolic outgases to escape from the part without damaging it. The porosity was measured using Quantachrome Ultrapyc 1200e automatic density analyzer.

SLS: Graphite

Graphite is well known for its high thermal stability and chemical inertness which renders it a good candidate for making refractory parts. The theoretical density of graphite is 2.25 g/cc which is relatively low compared to most metals. Figure 14 shows the SEM image of the GS 150E synthetic graphite powder obtained from Graftech Inc. It can be seen that it is very flaky in shape, rough and irregular in geometry. These surface characteristics actually make graphite difficult to process using powder metallurgy. The properties of graphite powder are tabulated in Table 6.

Table 6. Properties of GS 150E graphite powder

Property	Value
Specific gravity	2.25
Particle Size	(+/-2%) 83% < 75 microns
Cost	~$2.3/lb

Figure 14. SEM image of the synthetic graphite powder

Computer models for 25 mm cubic and 20 mm cylindrical disk graphite preforms were generated using ProEngineer Wilfire 3.0, and the .stl files obtained were loaded onto the Sinterstation 2000 software. The CAD models were generated taking into account the shrinkage that occurs during the high temperature furnace processing. The powder mixture was prepared by mixing graphite and phenolic resin in the ratio 7:3 by weight. The powder mixture was blended inside ball milling jars and allowed to mix for 6-8 hours at moderate speed. The mixed batch of powder was sifted to eliminate large sized particles and the grinding media and then the powder was loaded into both the feed bins of the sinterstation. The operating parameters used for sintering are tabulated in Table 7.

Table 7. Parameters used for graphite sintering

Parameter	Values
Powder composition	70 wt% graphite and 30 wt% phenolic resin
Laser power	20 W
Outline laser power	4 W
Scan speed	1.5 m/s
Beam diameter	450 μm
Scan spacing	76.2 μm
Layer thickness	101.6 μm
Part bed temperature	60°C
Feed Bin temperatures	45°C
Process gas	Inert gas, Nitrogen

Post Processing: Graphite

Post processing of the graphite preforms consisted of high temperature burnout of green parts to obtain the brown part. The temperature profile used for brown part formation was heating up the preform from room temperature to 200°C with a heating ramp rate of 60°C/hr, followed by slower ramp rate of 30°C/hr to 600°C, and then a 50°C/hr ramp rate cures the part to 1100°C. The dwelling time at the peak temperature was 1 hour. The part was left to cool back to room temperature naturally. The reason for slower heating ramp between 200°C and 600°C is to provide sufficient amount of time to allow the evolved gases to escape by diffusion through pores. In brown part formation it was observed that warping becomes a major issue as the heating ramp increases, due to

larger thermal gradients inside the part. Therefore, another reason for choosing a slower heating ramp was minimization of nonlinear geometric changes during the high temperature furnace processing. A slightly higher heating ramp between 600°C and 800°C is used since the amount of gases emitted during this stage is reduced. Research grade argon was filled into the chamber during the process to prevent oxidation of carbonized phenolic resins. The porosity was measured using Quantachrome Ultrapyc 1200e automatic density analyzer.

ELECTROCHEMICAL DEPOSITION

Sample Preparation: Silicon Carbide

Electrical conductivity of the material to be plated determines the density of the electronic charge cloud available on the surface of the material to reduce the metal ions to metals. Hence it plays an important factor in determining the success of the deposition process. The electrical conductivity of laser sintered silicon carbide is very low, around 10^{-6} S/cm; therefore, sample preparation plays an important role in its deposition process. Firstly the 25 mm cubic samples were cleaned in acetone for 15 minutes and then washed with distilled water to remove any unwanted impurities. Cleaning process was followed by activation and sensitization of the preform.

Silicon carbide preforms were sensitized by first dipping them in 1 L aqueous solution containing 10 g of tin chloride ($SnCl_2$) and 40 ml of concentrated hydrochloric acid (HCl) for 15 minutes, and then by washing them with distilled water. They were activated by placing them in 1 L aqueous solution containing 0.5 g of palladium chloride ($PdCl_2$) and 30 ml of concentrated hydrochloric acid (HCl) for 15 minutes followed by rinsing in distilled water. Finally, the preform was washed and rinsed thoroughly for 10-15 minutes with distilled water (Kretz, 2004 and Lee, 1996).

Sample Preparation: Graphite

Graphite samples were cleaned in acetone for 15 minutes and rinsed with distilled water. Heating them in atmospheric environment at 200°C activated cubic preforms. Graphite has a much higher electrical conductivity (200 S/cm) compared to silicon carbide, so sensitization was not mandatory. Still, electrochemical activation helps to get better yield of deposited metal, especially in the case of electroless plating.

Electroless plating

Electroless nickel plating was carried out at a pH of 9 and 80°C. The heat was supplied by putting the bath on top of a hot plate and the solution is agitated by means of a magnetic stirrer. The constituents of the electroless nickel plating in 1 L aqueous solution are tabulated in Table 8. The deposition process was carried out for 6 hours.

Table 8. Constituents of electroless nickel plating bath

Constituent	Salt	Weight	Supplier
Source	Nickel Sulphate Heptahydrate	45 g	Acros Ogranics
Reducing agent	Sodium Hypophosphite Monohydrate	8 g	Alfa Aesar
Complexing agent	Sodium Citrate Dihydrate	100 g	Fisher Scientific
Buffering agent	Ammonium Sulphate	50 g	Fisher Scientific

Electrolytic Deposition

Electrical connections were made by using the preform as a cathode and graphite as anode. The heat was supplied by putting the bath on top of a hot plate. The process was carried out at a pH of 3.5 and 48°C for 6 hours. The constituents of the electrolytic nickel plating in 1 L aqueous solution are tabulated in Table 9.

Table 9. Constituents of electrolytic nickel plating bath

Constituent	Salt	Weight	Supplier
Source	Nickel sulphate helptahydrate	225 g	Acros Organics
Source	Nickel chloride hexahydrate	37.5 g	Fisher Scientific
Buffering agent	Boric acid	30 g	Fisher Scientific

Modified Electrolytic Deposition

The electrical conductivity of silicon carbide is very low, so a sufficient electronic charge concentration was not achieved uniformly throughout the sample. This inhibited the oxidation of metal ions to form a metallic deposit. To overcome this, preforms used as the cathode were modified by inserting a conductive graphite electrode at the center of the silicon carbide preform in two configurations as shown in Figure 15 (Goel, 2009). The electrical conductivity of graphite is higher when compared to SiC. Thus a similar modified infiltration technique as SiC was applied to the graphite preforms with a copper rectangular cathode inserted at its center. The plating solution had the same composition

as the Watts bath mentioned in Table 9. The process was also carried out at the same conditions as electrolytic deposition, for 6 hours.

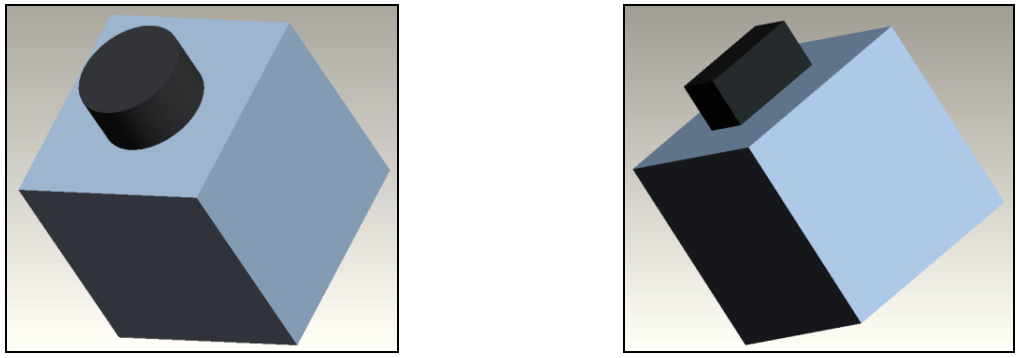

(a) (b)

Figure 15. Modified deposition: (a) cylindrical graphite cathode(b) rectangular graphite (SiC part) or copper (graphite part) cathode

The advantage of this modified process is postulated to be that the conductive cathode at the center will attract most of the metal ions through the pores. After the surface of these cathodes are completely saturated with the nickel metal deposits, and the reaction is still continued, the nickel metal will start depositing outwards on the pores and in this way a high part density can be achieved.

Forced Diffusion Deposition Method

A forced diffusion method was undertaken by forcing the electrolyte through the graphite sample using a high pressure bronze gear pump. A schematic of the forced diffusion method is shown in Figure 16(a) and a sample with the sample holder is shown in Figure 16(b).

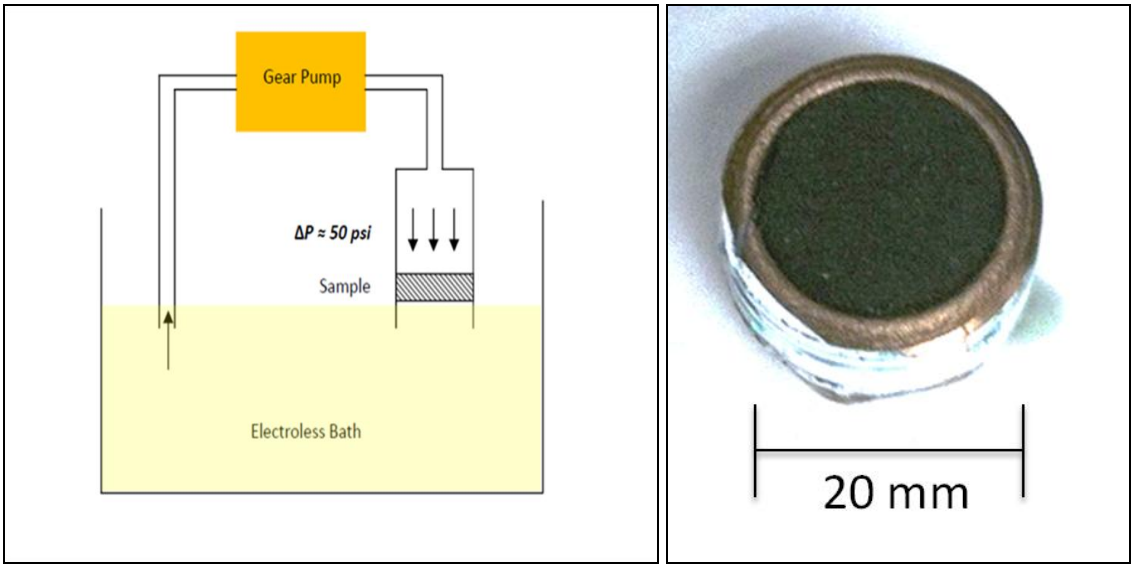

(a) (b)

Figure 16. (a) Schematic of forced diffusion process (b) Laser sintered graphite sample

The specifications of the Shurflo gear pump are tabulated in Table 10. No electrical connections were made to the sample. The whole setup for forced diffusion is shown in Figure 17. The sample was put inside the sample holder and the fluid (electroless bath electrolyte with the same composition and conditions as mentioned in Table 8) was pumped through the sample for 24 hours at a pressure of 50 psi. Prior to that, the viscosity of the electroless nickel plating solution was measure using the Cannon - Ubbelohde Viscometer. The kinematic viscosity was found by multiplying the efflux time with the viscometer constant (size 25 - 0.002 cSt/s). The average viscosity of the electroless nickel plating solution was computed to be 1.26 cSt.

Table 10. Specification of Shurflo GCBN23V gear pump

Output Power	0.5 HP
Voltage	115/230
Current	6.8/3.4
RPM	1725/1425
Maximum output pressure	125 psi
Maximum flow rate at max. pressure	2.4 gpm

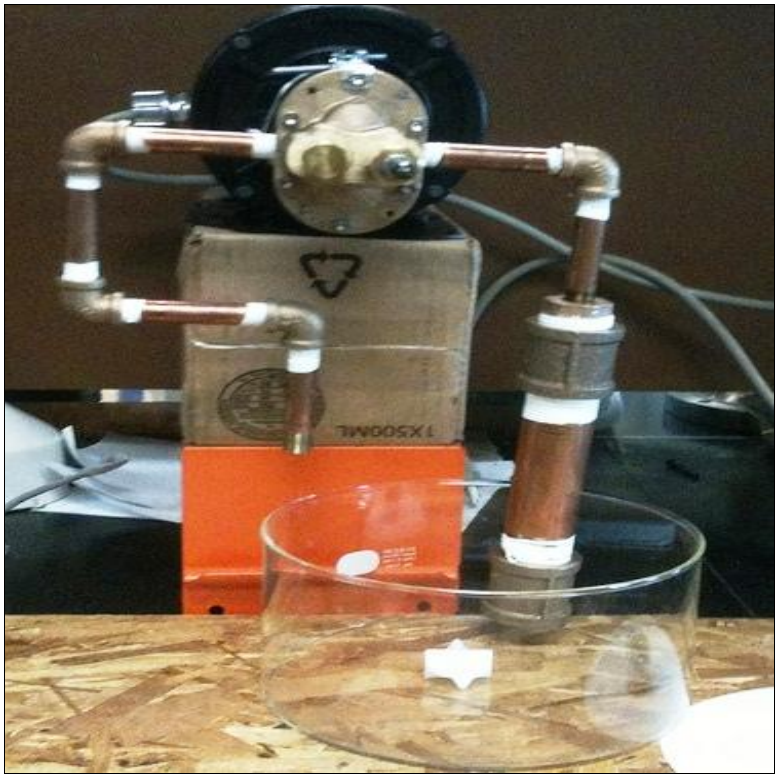

Figure 17. Forced diffusion deposition setup

After carrying out the deposition experiments, the parts were kept inside a convection oven at 150ºC for 2 hours to dry them for SEM analysis and to remove trapped fluids and gases. EDS maps were obtained using a JEOL-JSM 5610 SEM equipped with an Oxford Instruments EDS system. Figure 21 shows the image of the JEOL-JSM 5610 Scanning Electron Microscope.

Chapter 3: *Results*

POROSITY MEASUREMENT

Porosity of the brown parts were measured using the pychnometer. Table 11 shows the porosity measurements for laser sintered silicon carbide brown parts and Table 12 shows the porosity measurements for laser sintered graphite brown parts. The porosity reported by pychnometer is the open porosity.

Table 11. Pychnometer porosity measurements of SiC LS brown parts

Mass (g)	Apparent Volume (cc)	Apparent density (g/cc)	Porosity (%)
37.07	25.87	1.43	55.59
35.95	25.56	1.41	56.21
32.85	23.79	1.38	57.14
33.36	24.02	1.39	56.83
34.15	24.65	1.38	57.14
35.14	24.39	1.44	55.28
34.59	24.45	1.41	56.21
32.36	23.22	1.39	56.83

Table 12. Pychnometer porosity measurements of graphite LS brown parts

Mass (g)	Apparent Volume (cc)	Apparent density (g/cc)	Porosity (%)
20.07	21.26	0.94	58.22
19.36	20.31	0.95	57.78
21.35	21.70	0.98	56.44
21.07	21.20	0.99	56.00
19.86	20.41	0.97	56.89
20.35	20.29	1.00	55.56
20.88	21.25	0.98	56.44
20.25	20.89	0.97	57.89

Figure 18 shows an SEM image of the fractured surface of a 25 mm cubic silicon carbide brown part and Figure 19 shows SEM image of the fractured graphite brown part. The particles are bounded together by phenolic resin which got pyrolyzed to carbon after burn out at high temperature in the high temperature vacuum furnace.

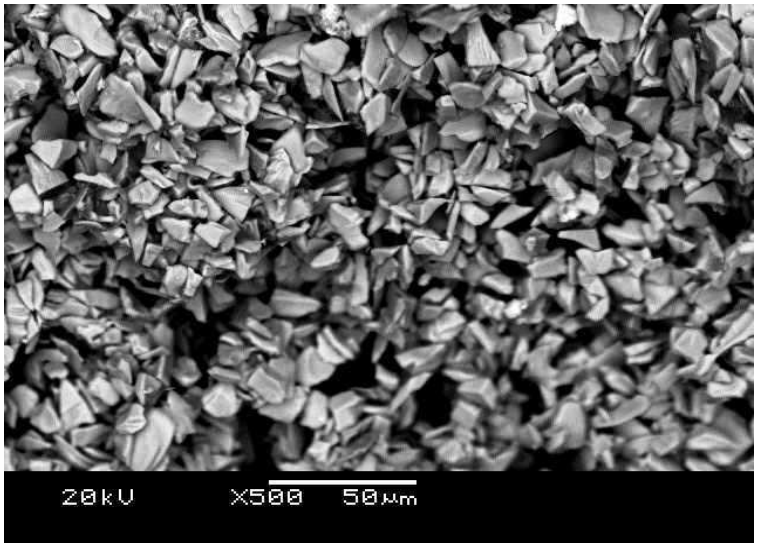

Figure 18. SEM image showing porous network in the SiC brown part

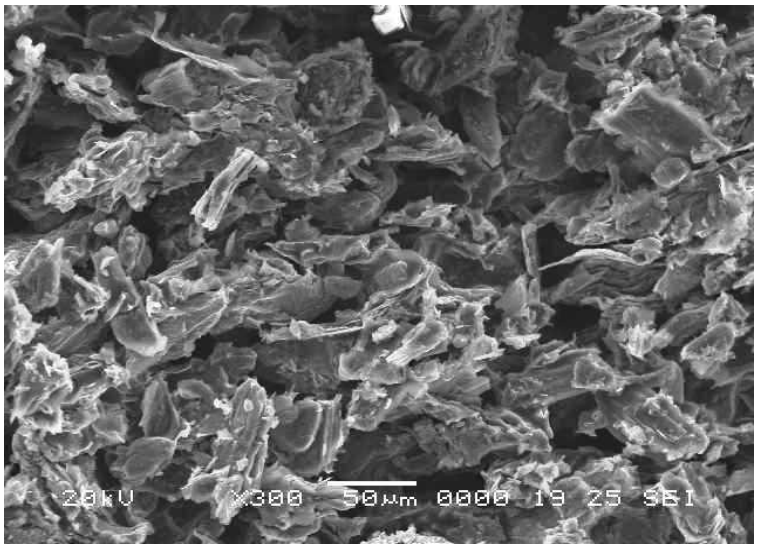

Figure 19. SEM image showing porous network in the graphite brown part

DEPOSITION: SEM AND EDS

Figure 20 shows an SEM image of the fractured cross section of a 25 mm silicon carbide cube after carrying out electroless deposition with nickel. Figure 21 shows an SEM image of the fractured silicon carbide cube after electrolytic deposition with nickel.

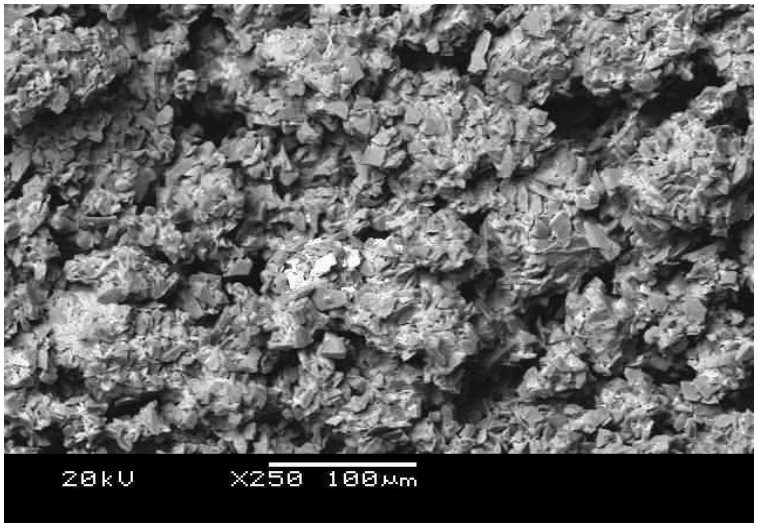

Figure 20. SEM image of a SiC preform after carrying out electroless nickel deposition

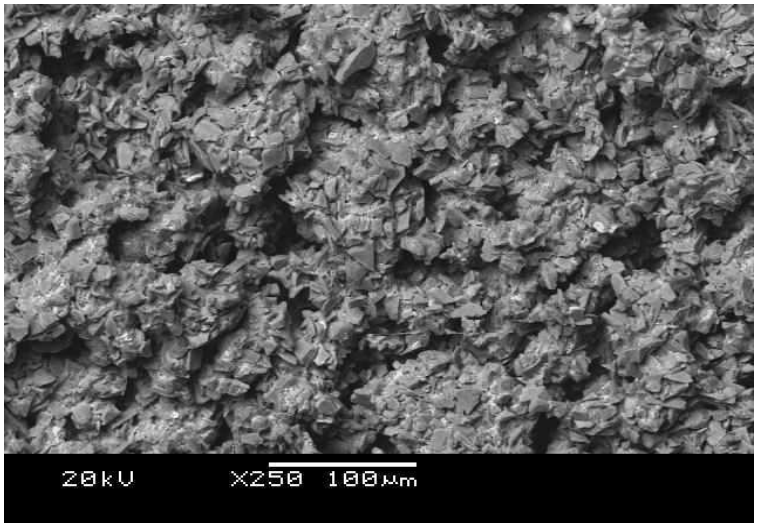

Figure 21. SEM image of a SiC part after carrying out electrolytic nickel deposition

Figure 22 shows an SEM image of the fractured cross section of a 25 mm silicon carbide cube after carrying out modified deposition with cylindrical cathode. Figure 23 shows an SEM image of the fractured silicon carbide cube after modified deposition with rectangular cathode.

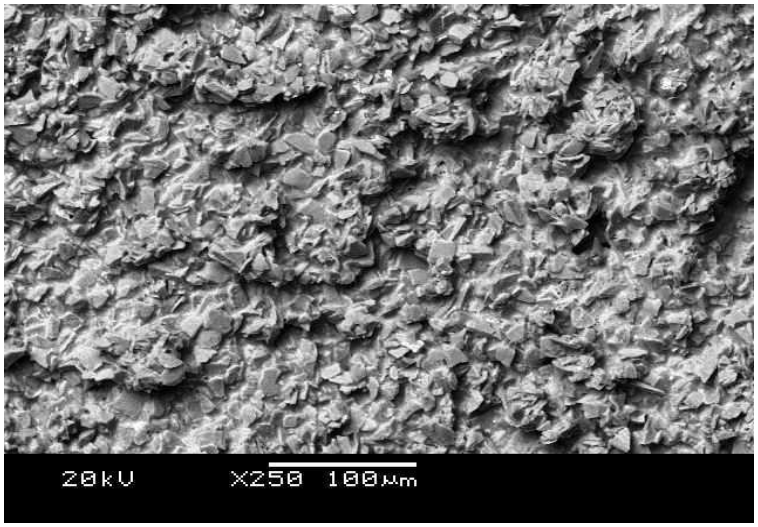

Figure 22. SEM image of a SiC part after modified deposition with cylindrical cathode

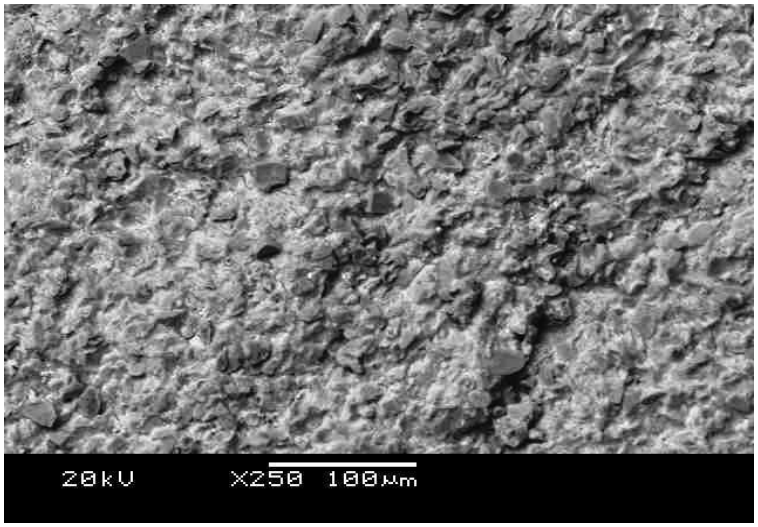

Figure 23. SEM image of a SiC part after modified deposition with rectangular cathode

Figure 24 shows an SEM image of the fractured cross section of a 25 mm graphite cube after carrying out modified deposition with rectangular copper cathode. Figure 25 shows an SEM image of the fractured graphite cylindrical disk after forced electroless deposition with nickel.

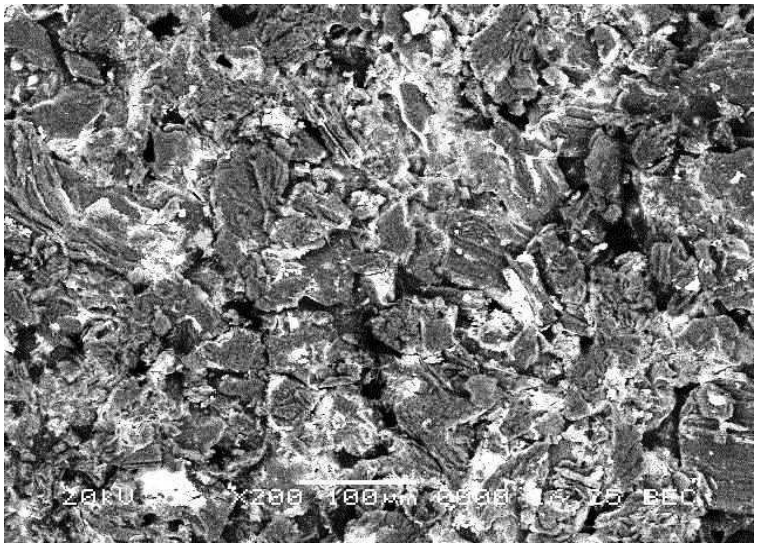

Figure 24. SEM image of a graphite part after modified deposition with rectangular copper cathode

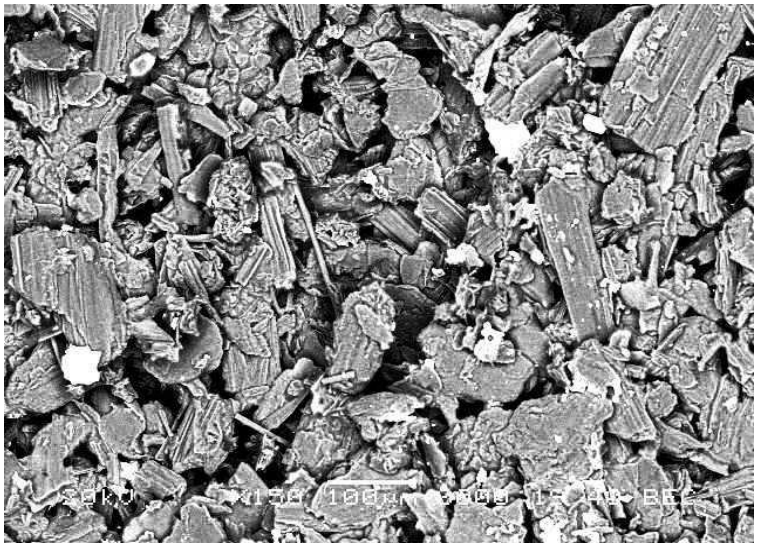

Figure 25. SEM image of a graphite part after forced electroless deposition

Figure 26 shows the EDS spectrum collected at fractured cross section of a 25 mm silicon carbide cube after carrying out electroless deposition with nickel. Figure 27 shows the EDS spectrum collected at fractured silicon carbide cube after electrolytic deposition with nickel.

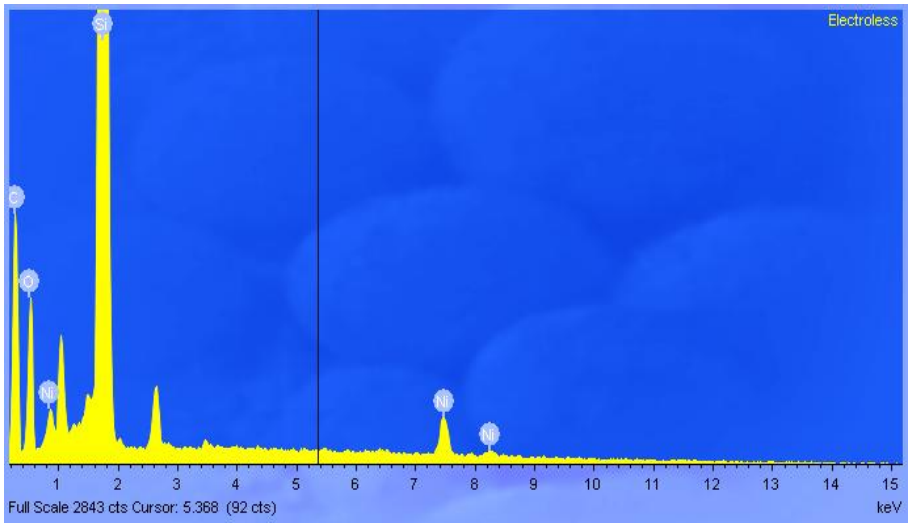

Figure 26. EDS spectrum for electroless deposition on SiC preforms

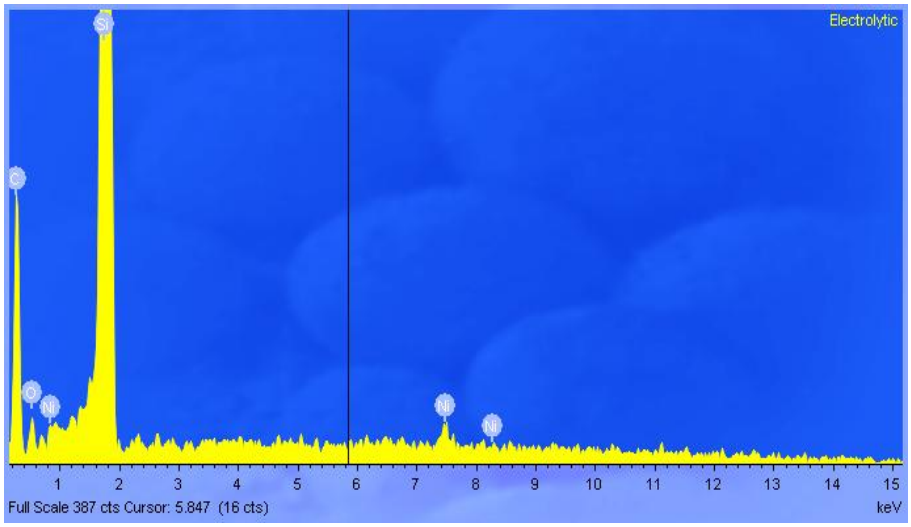

Figure 27. EDS spectrum for electrolytic deposition on SiC preforms

Figure 28 shows the EDS spectrum collected at fractured cross section of a 25 mm silicon carbide cube after carrying out modified deposition with cylindrical cathode. Figure 29 shows the EDS spectrum collected at fractured silicon carbide cube after modified deposition with rectangular cathode.

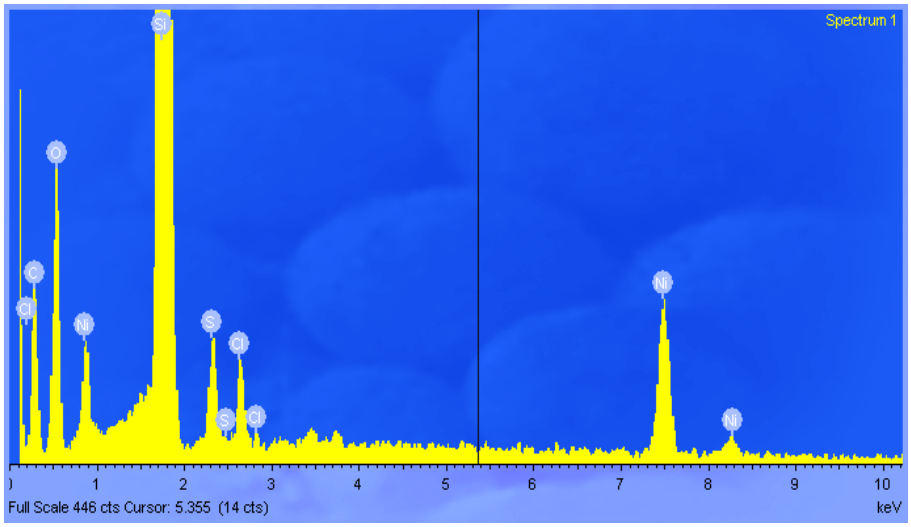

Figure 28. EDS spectrum for modified deposition on SiC preforms with cylindrical cathode

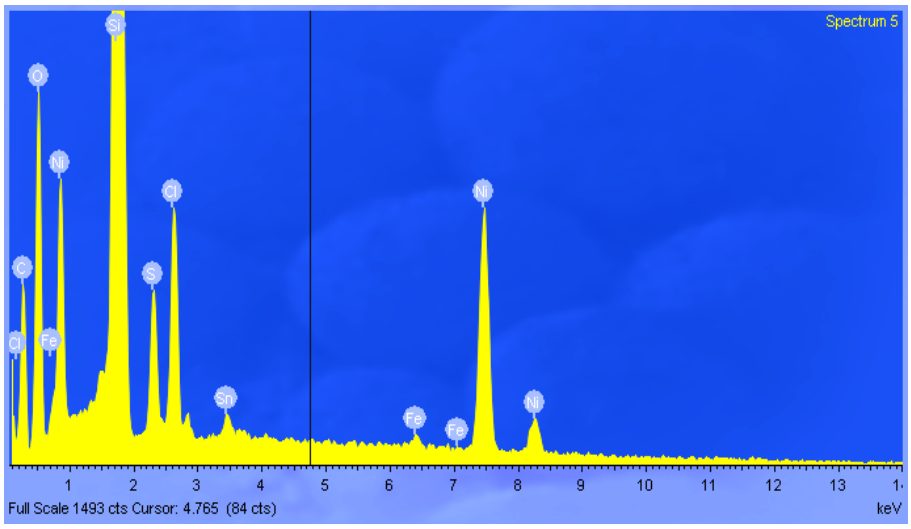

Figure 29. EDS spectrum for modified deposition on SiC preforms with rectangular cathode

Figure 30 shows the EDS spectrum collected at fractured cross section of a 25 mm graphite cube after carrying out modified deposition with rectangular copper cathode. Figure 31 shows the EDS spectrum collected at fractured graphite cylindrical disk after forced electroless deposition.

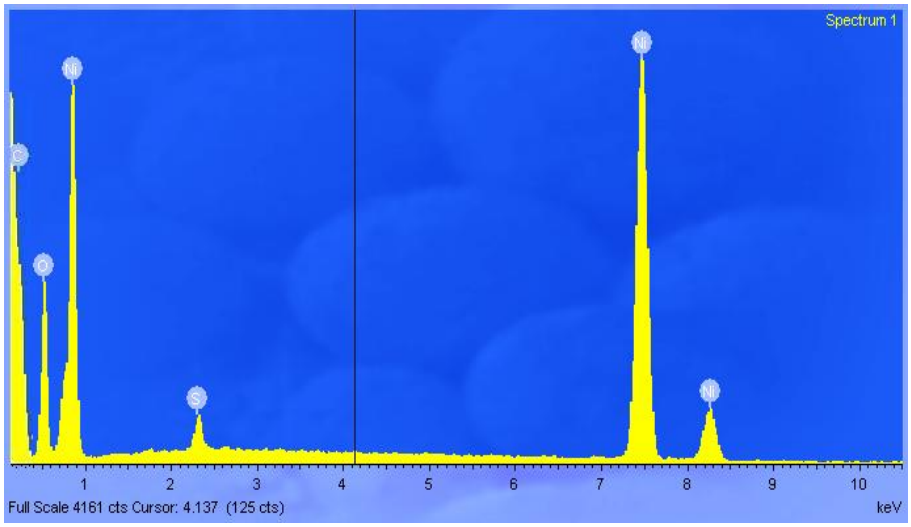

Figure 30. EDS spectrum for modified deposition on graphite preforms with rectangular copper cathode

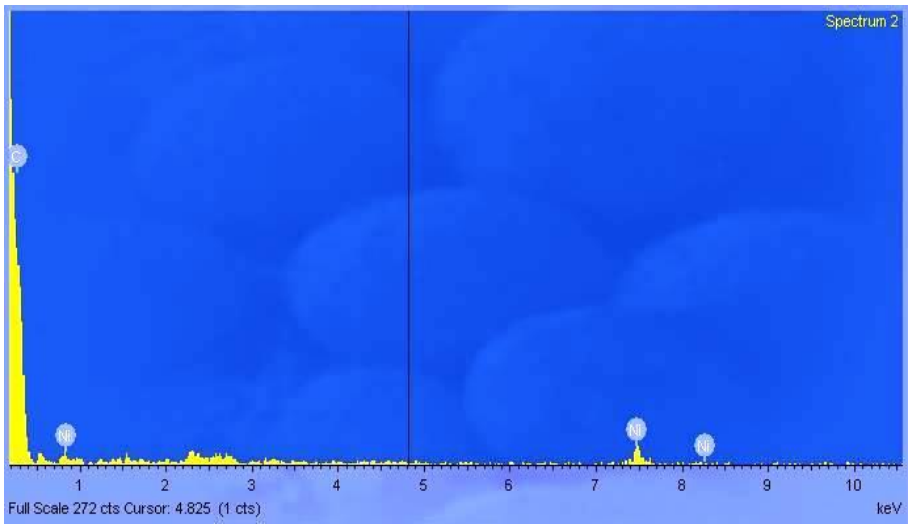

Figure 31. EDS spectrum for forced electroless deposition on cylindrical disk graphite preforms

Figure 32 shows the EDS map collected at fractured cross section of a 25 mm silicon carbide cube after carrying electroless deposition. Figure 33 shows the EDS map collected at fractured silicon carbide cube after electrolytic deposition with nickel. These maps were collected for 30 minutes.

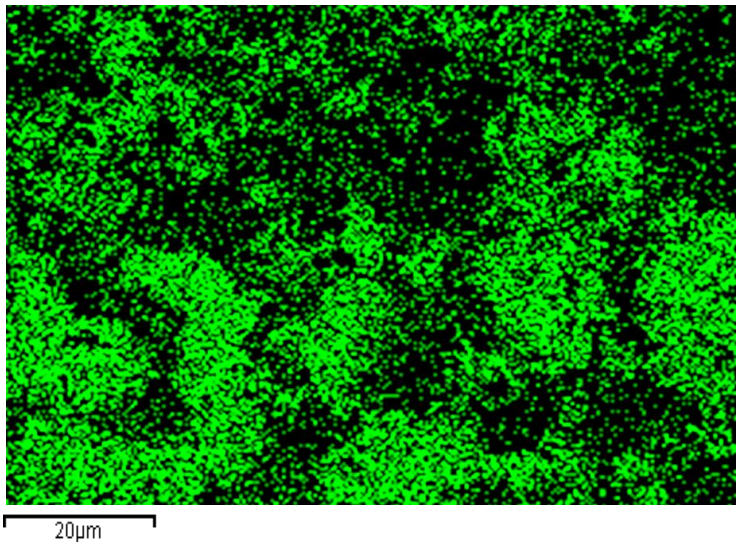

Figure 32. EDS map showing distribution of nickel after electroless deposition on SiC

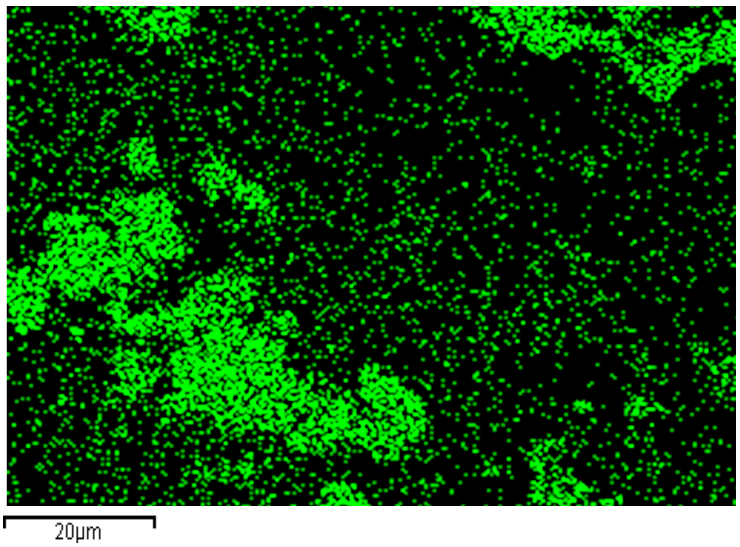

Figure 33. EDS map showing distribution of nickel after electrolytic deposition on SiC

Figure 34 shows the EDS map collected at fractured cross section of a 25 mm silicon carbide cube after carrying out modified deposition with cylindrical cathode. Figure 35 shows the EDS map collected at fractured silicon carbide cube after modified deposition with rectangular cathode. These maps were collected for 30 minutes.

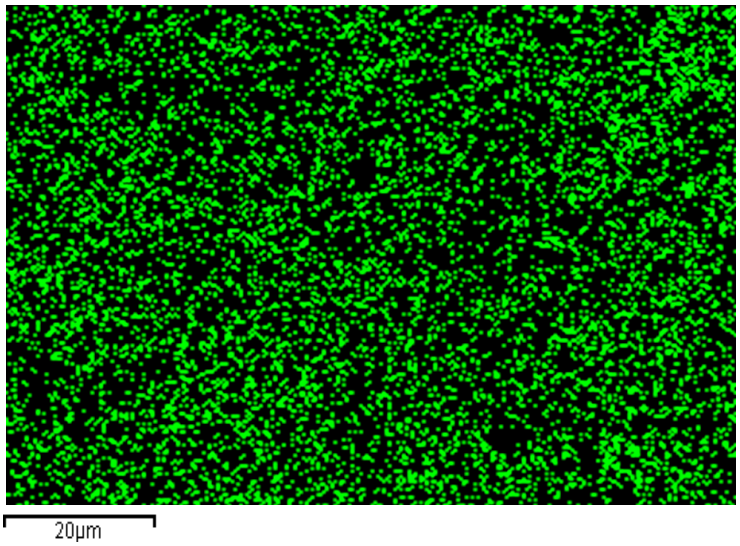

Figure 34. EDS map showing distribution of nickel after modified deposition with cylindrical cathode on SiC

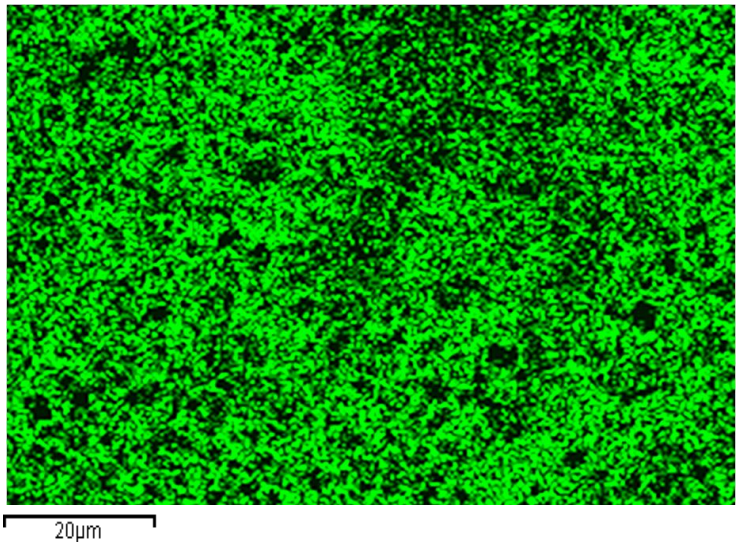

Figure 35. EDS map showing distribution of nickel after modified deposition with rectangular cathode on SiC

Figure 36 shows the EDS map collected at fractured cross section of a 25 mm graphite cube after carrying out modified deposition with rectangular copper cathode. Figure 37 shows the EDS map collected at fractured graphite cylindrical disk after forced electroless deposition. These maps were collected for 30 minutes.

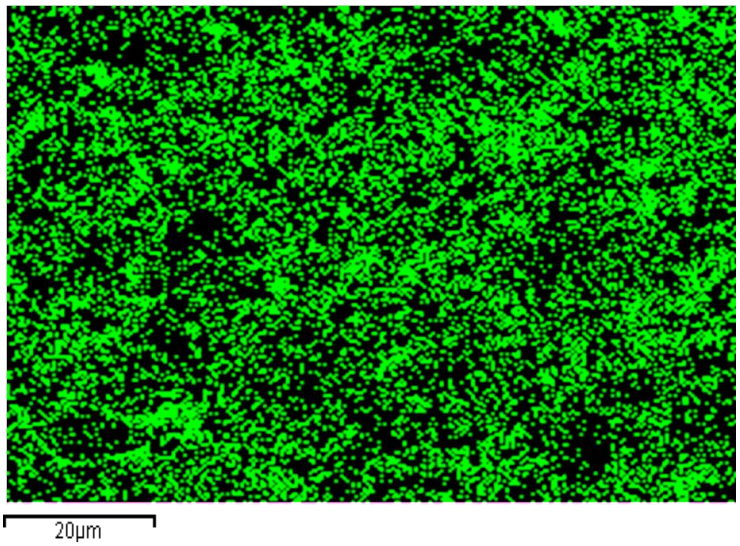

Figure 36. EDS map showing relative distribution of nickel after modified deposition with rectangular copper cathode on graphite

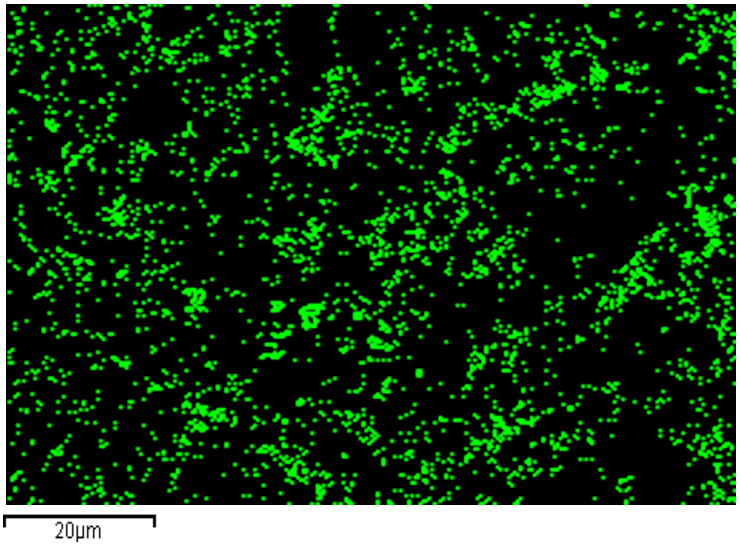

Figure 37. EDS map showing relative distribution of nickel after forced electroless deposition on graphite

Table 13 shows the weight percentage of nickel deposited in the pores inside the preform for each of the densification/deposition methods. The average weight percent of nickel was calculated by collecting EDS data at different regions and taking their mean.

Table 13. Weight percentage of nickel obtained after each deposition process

Process	Average % Nickel (by weight)
Electroless Deposition	6.4
Electrolytic Deposition	3.8
Modified Deposition SiC - Cylindrical Cathode	9.8
Modified Deposition SiC - Rectangular Cathode	18.6
Modified Deposition Graphite - Rectangular Cathode	16.6
Forced Diffusion Method	6.2

ENERGY CONSIDERATIONS

Table 14 shows the comparison between various infiltration processes in terms of energy consumption.

Table 14. Energy comparison for various kinds of deposition process

Process	Estimated Power Consumption(kW)
Vacuum Melt Infiltration	12-18
Electrochemical Deposition	0.7-0.9
Forced Electroless Deposition	0.8-1.6
Chemical Vapor Infiltration	4-8

Chapter 4: *Discussion*

POROSITY MEASUREMENT

Pychnometry gives only the open porosity inside the parts. The results show that average porosity in the parts can be assumed to be around 55 ~ 57%. This means that in a 25 mm cubic preform (volume 1 in^3), approximately 0.55 ~ 0.57 in^3 is an interconnected network of pores. There is some closed porosity which can also be estimated, but that is not of much interest since it is practically impossible to deposit on closed pores.

SEM images of the brown part roughly give an idea about the size of the pores. By comparing with the scale, it can be roughly estimated that the average pore size in silicon carbide parts is about 55 μm. The silicon carbide particles are bounded together by carbonized phenolic. For graphite, using the SEM image of its brown part, it can be estimated that the average pore size is around 50 μm.

DEPOSITION: SEM AND EDS

Figure 20 shows the backscatter electron (BSE) images of the fractured cross section of the silicon carbide after carrying out electroless deposition. In case of electroless deposition in silicon carbide preforms, several bright white patches could be seen which are from Sn-Pd clusters used for surface treatment before carrying out the process. Since tin and palladium have very high atomic number compared to silicon and carbon, they appear as bright white patches on the backscatter electron image. The atomic number of nickel is 28, which is quite close to silicon (atomic number 14); hence, the contrast difference between nickel and silicon is not large. The dispersed non-uniform shade of white which can be seen is nickel. It can also be deduced that the pores are not completely covered, and few pores can still be seen in Figure 20. Figure 26 shows the EDS spectrum for the electroless deposition. The major elements are nickel, silicon,

carbon and oxygen. The presence of oxygen can be explained due to the formation of nickel oxides. The EDS map for the electroless deposition shows that the deposition is not uniform. This might be due to the non-uniformity in the pore shape and size. Another reason could be that most of the nickel was deposited on the surface of the preform thereby blocking the pore openings on the surface and preventing further diffusion of ions inside the preform. The average percentage of nickel concentration (by weight) deposited inside the pores, in electroless deposition, was 6.4 percent as shown in Table 13.

For electrolytic deposition, as seen in Figure 21 there are no bright spots on the BSE image, since the samples were not treated with tin and palladium before carrying out the deposition. A lot of uncovered pores can be seen and contrast coming from nickel is also very dim and non uniform. Major elements seen in the EDS spectrum (Figure 27) are silicon, carbon, nickel and oxygen. The nickel peak is also very low compared to electroless deposition. The presence of oxygen again can be attributed to the formation of nickel oxides. The EDS map (Figure 33) shows the non-uniformity in the concentration of nickel deposited. This might be due to incomplete depletion of ions inside the pores. Due to the very low conductivity of silicon carbide and the non-catalytic surface, the electronic charge was not sufficient to reduce the nickel cations to deposit nickel metal. The average weight percent of nickel for this case was much poorer than electroless deposition and was found to be only 3.8 percent.

Figures 22 and 23 show the BSE images of the novel modified methods of deposition assessed in this research; cylindrical conductive cathode (Figure 22) and rectangular conductive cathode (Figure 23). It can be seen clearly from the BSE images and the EDS maps (Figures 34 and 35) that the distribution of deposited nickel is more or less uniform but density is much higher in case of the rectangular cathode compared to

the cylindrical cathode approach. This is because the rectangular cathode provided a larger surface area for ion deposition, especially on one side of the electrode which was parallel and facing the anode. The rate of deposition was faster on this side compared to the other side. As a result, a greater amount of nickel was deposited on the walls. Orientation of the two electrodes does matter in case of electrochemical deposition which can be easily resolved by using two anodes on either side of the rectangular cathodic preform. EDS spectra of both these processes (Figures 28 and 29) show that the major elements were silicon, carbon, nickel and oxygen. Presence of chlorine and sulphur can be due to the trapped electrolytes inside which eventually lead to the formation of sulphates and chlorides. Oxygen is present due to the formation of nickel oxide. Presence of trace amounts of iron in case of rectangular cathode deposition cannot be explained. As far as the average weight percent of deposited nickel goes, there was a significant improvement when compared to electroless and electrolytic methods. The average weight percent of nickel was measured to be 9.8 percent for cylindrical cathode deposition and 18.6 percent for rectangular cathode deposition. The maximum weight percent of nickel was found to be 22.6 percent for rectangular cathode deposition.

Similarly for graphite, modified deposition was performed by inserting a more conductive rectangular copper cathode at its center. It can be seen from the BSE image (Figure 24) and EDS map (Figure 36) that nickel is quite uniformly deposited inside the pores. The average weight percent of deposited nickel was found to be 16.6 percent. This value is a little lower than rectangular cathode deposition of silicon carbide because graphite has a much higher electrical conductivity and some deposition also took place on the surface thereby blocking the pores for further diffusion of ions inside the pore network. The associated EDS spectrum (Figure 30) shows that major elements were

carbon, nickel and oxygen. Nickel is deposited as nickel oxide which gives rise to oxygen peaks in the spectrum.

Due to the nature of the geometry where the radius of the pore is much smaller than the length of the pore, it can be assumed that the mass transfer is dominated by diffusion. That motivated the external forced diffusion method. This method did not perform well as compared to the modified processes since the applied pressure was too high. BSE image (Figure 25) show only globs of bright patches which are from chlorate and sulphate complexes due to trapped electrolyte. Although the deposition is more uniform compared to electroless deposition of silicon carbide, the density is poor, and the average weight percent of deposited nickel is 6.2 percent, which shows no improvement in comparison to electroless deposition without forced diffusion. Better pressure control coupled with modified electrolytic deposition has the potential to give improved infiltration and deposition simultaneously. Nickel peaks from the EDS spectrum (Figure 31) are barely distinguishable compared to other processes.

ENERGY CONSIDERATIONS

The work being carried out also leads to minimization of energy consumption in the post-processing stage as compared to other infiltration techniques such as vacuum or melt infiltration. In turn this will result in reducing the overall post-processing cost in creating fully dense parts. It was found that the commercial vacuum melt infiltration process consumes approximately 45 MJ of energy per hour at 240 V and 50 A to maintain a temperature of about 1000°C. In turn it also consumes around 35 gallons of water per minute to cool the furnace down from 1000°C to room temperature. The current process of electrochemical infiltration uses a very little amount of energy and hence is very cost-effective as well. The major source of energy consumed in the

electroless and electrolytic processes is from the hot plate. Forced diffusion method used more energy since power is needed to drive the motor of the pump. But still, the energy consumed by the electrochemical process is at least 15 times lower than for the vacuum melt infiltration method.

Chapter 5: *Summary, Conclusions and Future Work*

SUMMARY

In this research the feasibility to infiltrate laser sintered porous preforms with metals at room temperature was demonstrated. This was achieved by developing a truly novel densification process by modifying the electrodeposition process. This densification process carries out diffusion of metals ions into the porous structure and deposition on walls of the pores simultaneously. Both conductive and non-conductive preforms may be electrochemically infiltrated, and MMCs produced by this method have potential for use in structural applications. Electrochemical deposition methods explored included electroless infiltration, electrolytic infiltration and forced diffusion methods. Graphite-nickel and silicon carbide-nickel were two material systems assessed for this work. Electrodeposition methods such as electroless deposition and electrolytic deposition methods were tried. These processes were modified by inserting a more conductive cathode plate at the center of the porous sample. The results achieved were encouraging. EDS analysis, after the infiltration, demonstrated that approximately 20% of nickel by weight was deposited in the pores. The work being carried out also leads to minimization of energy consumption in the post-processing stage as compared to other infiltration techniques such as vacuum or melt infiltration. In turn this will result in reducing the overall post-processing cost in creating fully dense parts. It was also found that the vacuum melt infiltration process consumes approximately 12kWh of energy at 240 V and 50 A to maintain a temperature of about 1000°C. The current process of electrochemical infiltration uses a very little amount of energy around 0.7-1.2 kWh and therefore is very cost-effective as well.

CONCLUSIONS

Electrochemical infiltration of laser sintered preforms with metal has been shown to be feasible with the potential to produce fully dense parts. One of the major drawbacks of non-polymeric SLS technology has been high porosity. This research enables production of high-density parts without any undesirable structural and chemical changes. Of several deposition techniques surveyed, modified electrolytic infiltration with a rectangular cathode performed best for both silicon carbide and graphite. The novel process described in this article is potentially more energy efficient compared to the state of the art vacuum-melt infiltration technique. One of the major challenges faced in this research relates to the depletion of desired ions into the small pores (where the solution is not assumed to be well-stirred). While the results show incomplete closure of the void network, they are nonetheless encouraging since a significant amount of nickel was deposited deep within the pores network. Deposition infiltration of freeform fabricated parts is shown to maintain dimensional stability of the part and to enable freeform creation of functional parts. This work would enable faster transition of SLS from rapid prototyping to a rapid manufacturing technique. This would prove to be more useful in fabrication of parts with complex geometry and small dimensions.

FUTURE WORK

Future work includes exploring other deposition techniques and comparison of those results to these. Ionic diffusion affects the infiltration process to a great extent, so methods having enhanced diffusion rates such as pressurized diffusion of electrolyte into the preform need to be assessed. Other techniques include electrophoretic infiltration in which the charged ions move relative to the electrolyte, through the porous network under the action of applied field. Electroosmotic methods can also be tried where the electrolyte moves with respect to the stationary charged surface. Another important issue

is identification of a method for driving the trapped gases and electrolyte out of the porous structure. It is very essential to go deeper into the physics of the problem and develop a mathematical model which can be used to find optimal parameters for carrying out the process and correlate the experimental data.

Bibliography

Alayavalli, K. and Bourell, D.L., "Fabrication of modified graphite bipolar plates by indirect selective laser sintering (SLS) for direct methanol fuel cells", *Rapid Prototyping Journal* 16, No. 4 (2010), pp.268 - 274

Bari, G.D., "Nickel Plating", *Surface Engineering* 5 (1994), pp. 201

Besmann, T.M., Lowden, R.A., Sheldon, B.W. and Stinton, D.P., "Chemical Vapor Infiltration", *Proceedings of Electrochemical Society* 90-12 (1990), pp. 482-491

Biggar, G.M., "The ionic radius of nickel", *Minerological Magazine* 37 (1969), pp. 286

Bourell, D.L., Beaman, J.J., Marcus, H.L. and Barlow, J.W., "Solid freeform fabrication: an advanced manufacturing approach", *Proceedings of the Solid Freeform Fabrication Symposium* (1990), pp. 1-7

Burns, R, and E W Orrel. "A Thermal Analytical Study of Phenol Formaldehyde Resins" *Journal of Material Science* 2 (1967), pp. 72-77

Chen, L.F., Luo, X.T. and Wu, Q.L., "Electrochemical preparation of fiber reinforced metallic matrix composites", *Journal of Materials Science Letters* 23 (2003), pp. 379-381

Chiou, J.M. and Chung, D.D.L., "Characterization of metal matrix composites fabricated by vacuum infiltration of liquid metal under an inert gas pressure", *Journal of Materials Science* 26 (1991), pp 2583-2589

Davis, J.R., "*Copper and copper alloys*", ASM International, 2001

Deckard, C., "Method and Apparatus For Producing Parts By Selective Sintering", *US Patent*, 4863538, 1986

Dieringa, H., Hort, N. and Kainer, K.U., „Magnesium Based MMCs Reinforced with C-Fibers", *The AZo Journal of Materials online* (2005), pp. 1-10

Duck, J., Niebling, F., Neeβe, T. and Otto, A., "Infiltration as post-processing of laser sintered metal parts", *Journal of Powder Technology* 145 (2004), pp. 62-68

Dutta, S., "Sinterability, strength and oxidation of alpha silicon carbide powders", *Journal of Materials Science* 19, No. 4, pp. 1307-1313

Esfehanian, M., Heinrich, J.G., Horvath, J., Koch, D. and Grathwohl, G., "Silicide-carbide composites obtained from alloyed melt infiltration", *Journal of Materials Science* 42 (2007), pp. 7721-7728

Evans, R.S., Bourell, D.L., Beaman, J.J. and Campbell, M.I., "Rapid manufacturing of silicon carbide composites", *Rapid Prototyping Journal* 11, No. 1 (2005), pp. 37-40

Ghomashchi, M.R. and Vikhrov, A., "Squeeze casting: an overview", *Journal of Materials Processing Technology* 101, No. 1-3 (2000), pp. 1-9

Goel, A. and Bourell, D.L., "Electrochemical Infiltration of Selective Laser Sintered Preforms with Metals", *Proceedings of the Solid Freeform Fabrication Symposium* (2009), pp. 332-341

Hasegawa, T., et al, "Micro-flow control and Micropump by applying electric fields through a porous membrane", *JSME International Journal* 47, No. 3 (2004), pp. 557-563

Jain, C.C., Wang, S.S., Chuang, T.H. and Yang, S.R., "Low Temperature Direct Electroless Nickel Plating on Silicon Wafer, *Journal of the Chinese Institute of Engineers* 32, No. 1 (2009), pp. 137-140

Kanani, N., "*Electroplating: basic principles, processes and practice*", Elsevier, 2004

Koh, J.C.Y. and Fortini, A., "Prediction of thermal conductivity and electrical resistivity of porous metallic materials", *International Journal of Heat Mass Transfer* 16 (1973), pp. 70-76

Kretz, F., Gàcsi, Z., Kovàcs, J. and Pieczonka, T., "The electroless deposition of nickel on SiC particles for aluminum matrix composites", *Journal of Surface and Coatings Technology* 180-181 (2004), pp. 575-579

Kruth, J.P. et al., "Basic Powder Metallurgical Aspects in Selective Metal Powder Sintering," *Annals of the CIRP* 45, No. 1 (1996), pp. 183–186

Kumar, S., "Selective Laser Sintering: A Qualitative and Objective Approach", *Journal of Materials Science* 55, No. 10 (2004), pp. 43-47

LeBlanc, O.H., "Electroless nickel plating composition and method for its preparation and use", *US Patent*, 4780342, 1988

Lee, T.J., Sheppard, K.G., Li, Y.Q. and Gallois, B., "Synthesis of a nanophase, whisker-reinforced, ceramic/metal composite by electrochemical infiltration", *Journal of Materials Science* 31 (1996), pp. 6555-6563

Lou, H.H. and Huang, Y. "Electroplating", *Encyclopedia of Chemical Processing* (2006), pp. 1-10

Madar, R., "Materials science: Silicon carbide in contention", *Nature* 430 (2004), pp. 974-975

Mallory, G.O., "*Electroless plating: fundamentals and applications*", Cambridge University Press, 1991

Mantell, C.L., "*Carbon and Graphite Handbook*", Interscience Publishers, 1979

Marton, J.P. and Schlesinger, M., "The nucleation growth and structure of thin Ni–P films" *Journal of Electrochemical Society* 115, No. 1 (1968), pp. 16–21

Mortensen, A., Marchi, C.S. and Degischer, H.P., "Glossary of terms Specific to Metal Matrix Composites, *MMC Assess Consortium* (2010), pp. 1-13

Paunovic, M. and Schlesinger, M., "*Fundamentals of Electrochemical Deposition*", 2nd Edition, Wiley, 2006

Rubinstein, I., "Electro-diffusion of ions", SIAM, 1990

Saleh, N., et al, "Effect of electroplating on mechanical properties of stereolithography and laser sintered parts", *Rapid prototyping Journal* 10, No. 5 (2004), pp. 305-315

Sen, D., et. al, "Investigation on pore structure and small-scale agglomeration behavior in liquid phase sintered SiC using small angle neutron scattering", *PRAMANA-Journal of Physics* 71, No. 5 (2008), pp. 979-984

Somiya, S., "*Silicon Carbide Ceramics: Fundamental and solid reaction*", Springer 1991

Stevinson, B., "Support free infiltration of selective laser sintered (SLS) silicon carbide preforms", *M. S. E Thesis*, The University of Texas at Austin

Streckert, H.H., et. al, "Microwave densification of electrophoretically infiltrated silicon carbide composite", *Journal of Materials Science* 32 (1997), pp. 6429-6433

Subramanian, K., Vail, N., Barlow, J.W. and Marcus, H.L., "Selective laser sintering of alumina with polymer binders", *Rapid Prototyping Journal* 1, No. 2 (1995), pp. 24-35

Vallabhajosyula, P. and Bourell, D.L., "Selective Laser Sintering and Post Processing of Fully Ferrous Components", *Proceedings of the Solid Freeform Fabrication Symposium* (2008), pp. 179-185

Wang, J.C., "Young's modulus of porous materials", *Journal of Materials Science* 19, No. 3 (1984), pp. 801-808

Xu, C., Li, M., Zhang, X., Tu, K. and Xie, Y., "Theoretical studies of displacement deposition of nickel into porous silicon with ultrahigh aspect ratio", *Electrochimica Acta* 52 (2006), pp. 3901–3909

Xu, C., Zhang, X., Tu, K. and Xie, Y., "Nickel Displacement Deposition of Porous Silicon with Ultrahigh Aspect Ratio", *Journal of the Electrochemical Society* 153, No. 3 (2007), pp. D170-D174

Zhang, X., et. al, "Pulse Electroplating of Copper Film: A Study of Process and Microstructure", *Journal of Nanoscience and Nanotechnology* 8 (2008), pp. 2568–2574

Zhao, H.B., Pflanz, K., Gu, J.H., Li, A.W, Stroh, N., Brunner, H. and Xiong, G.X., "Preparation of Palladium composite membranes by modified electroless plating procedure", *Journal of Membrane Science* 142 (1998), pp. 147-157

Vita

Abhishek Goel was born in Kolkata, India on February 9, 1986, the son of Prem Chand Goel and Saroj Devi Goel. He completed his high school at Haryana Vidya Mandir, Kolkata, India in 2004 and graduated from Indian Institute of Technology, Kharagpur, India with his Bachelor's degree (Hons.) in Manufacturing Science and Engineering in 2008. He has always been interested in non-conventional manufacturing processes and its related research. In August, 2008, he entered the Graduate School at the University of Texas at Austin.

Abhishek loves creation and hopes to build and create something soon for the benefit of mankind. He loves to read books, solve mathematical puzzles and play billiards.

Permanent Address: 24/4/1A, Ramkrishna Samadhi Road
Kankurgachi, Kolkata
West Bengal, India – 700054
Ph: + 91 –33 23629824
Email: goelabhishek86@gmail.com

This thesis was typed by Abhishek Goel.